



International Agreement Report

TRACE Nodalization Performance in PSB-VVER SB-LOCA Benchmark

Prepared by:
R. Orosz, T. Varju, B. Biró & A. Aszódi

Budapest University of Technology and Economics
Institute of Nuclear Techniques
Műegyetem rkp. 3.
1111 Budapest, Hungary

A. Hsieh, NRC Project Manager

**Division of Systems Analysis
Office of Nuclear Regulatory Research
U.S. Nuclear Regulatory Commission
Washington, DC 20555-0001**

Manuscript Completed: May 2025
Date Published: July 2025

Prepared as part of
The Agreement on Research Participation and Technical Exchange
Under the Thermal-Hydraulic Code Applications and Maintenance Program (CAMP)

**Published by
U.S. Nuclear Regulatory Commission**

AVAILABILITY OF REFERENCE MATERIALS IN NRC PUBLICATIONS

NRC Reference Material

As of November 1999, you may electronically access NUREG-series publications and other NRC records at NRC's Library at www.nrc.gov/reading-rm.html. Publicly released records include, to name a few, NUREG-series publications; *Federal Register* notices; applicant, licensee, and vendor documents and correspondence; NRC correspondence and internal memoranda; bulletins and information notices; inspection and investigative reports; licensee event reports; and Commission papers and their attachments.

NRC publications in the NUREG series, NRC regulations, and Title 10, "Energy," in the *Code of Federal Regulations* may also be purchased from one of these two sources.

1. The Superintendent of Documents

U.S. Government Publishing Office
Washington, DC 20402-0001
Internet: <https://bookstore.gpo.gov/>
Telephone: (202) 512-1800
Fax: (202) 512-2104

2. The National Technical Information Service

5301 Shawnee Road
Alexandria, VA 22312-0002
Internet: <https://www.ntis.gov/>
1-800-553-6847 or, locally, (703) 605-6000

A single copy of each NRC draft report for comment is available free, to the extent of supply, upon written request as follows:

Address: **U.S. Nuclear Regulatory Commission**
Office of Administration
Digital Communications and Administrative
Services Branch
Washington, DC 20555-0001
E-mail: Reproduction.Resource@nrc.gov
Facsimile: (301) 415-2289

Some publications in the NUREG series that are posted at NRC's Web site address www.nrc.gov/reading-rm/doc-collections/nuregs are updated periodically and may differ from the last printed version. Although references to material found on a Web site bear the date the material was accessed, the material available on the date cited may subsequently be removed from the site.

Non-NRC Reference Material

Documents available from public and special technical libraries include all open literature items, such as books, journal articles, transactions, *Federal Register* notices, Federal and State legislation, and congressional reports. Such documents as theses, dissertations, foreign reports and translations, and non-NRC conference proceedings may be purchased from their sponsoring organization.

Copies of industry codes and standards used in a substantive manner in the NRC regulatory process are maintained at—

The NRC Technical Library

Two White Flint North
11545 Rockville Pike
Rockville, MD 20852-2738

These standards are available in the library for reference use by the public. Codes and standards are usually copyrighted and may be purchased from the originating organization or, if they are American National Standards, from—

American National Standards Institute

11 West 42nd Street
New York, NY 10036-8002
Internet: www.ansi.org
(212) 642-4900

Legally binding regulatory requirements are stated only in laws; NRC regulations; licenses, including technical specifications; or orders, not in NUREG-series publications. The views expressed in contractor prepared publications in this series are not necessarily those of the NRC.

The NUREG series comprises (1) technical and administrative reports and books prepared by the staff (NUREG-XXXX) or agency contractors (NUREG/CR-XXXX), (2) proceedings of conferences (NUREG/CP-XXXX), (3) reports resulting from international agreements (NUREG/IA-XXXX), (4) brochures (NUREG/BR-XXXX), and (5) compilations of legal decisions and orders of the Commission and Atomic and Safety Licensing Boards and of Directors' decisions under Section 2.206 of NRC's regulations (NUREG-0750), and (6) Knowledge Management prepared by NRC staff or agency contractors.

DISCLAIMER: This report was prepared under an international cooperative agreement for the exchange of technical information. Neither the U.S. Government nor any agency thereof, nor any employee, makes any warranty, expressed or implied, or assumes any legal liability or responsibility for any third party's use, or the results of such use, of any information, apparatus, product or process disclosed in this publication, or represents that its use by such third party would not infringe privately owned rights.



International Agreement Report

TRACE Nodalization Performance in PSB-VVER SB-LOCA Benchmark

Prepared by:
R. Orosz, T. Varju, B. Biró & A. Aszódi

Budapest University of Technology and Economics
Institute of Nuclear Techniques
Műegyetem rkp. 3.
1111 Budapest, Hungary

A. Hsieh, NRC Project Manager

**Division of Systems Analysis
Office of Nuclear Regulatory Research
U.S. Nuclear Regulatory Commission
Washington, DC 20555-0001**

Manuscript Completed: May 2025
Date Published: July 2025

Prepared as part of
The Agreement on Research Participation and Technical Exchange
Under the Thermal-Hydraulic Code Applications and Maintenance Program (CAMP)

**Published by
U.S. Nuclear Regulatory Commission**

ABSTRACT

In the recent decades computer code calculations have become invaluable in nuclear engineering. With the modern tools, the experts are able to predict the different processes with high accuracy, which has numerous advantages, such as improved reactor safety, enhanced design optimization and cost-effectiveness. It is however essential that the user possesses adequate knowledge and experience about the given code, including its principles and limitations.

In the current report the focus is on the nodalization of the thermal-hydraulic models built for the PSB-VVER integral test facility. Altogether three models have been constructed in TRACE, where the main differences are in the used components and their nodalization of the RPV section. To assess the behavior of the models, a cold leg small break loss of coolant accident benchmark was chosen. In the report we present both the qualitative and quantitative comparison of the calculations and the measurements performed on the facility. For the quantitative evaluation, two methods, namely FFTBM-SM and SARBM, have been used. Finally, a summary of the notable observations and recommendations is included.

TABLE OF CONTENTS

ABSTRACT	iii
TABLE OF CONTENTS.....	v
LIST OF FIGURES.....	vii
LIST OF TABLES	ix
ACKNOWLEDGMENTS	xi
ABBREVIATIONS AND ACRONYMS	xiii
1 INTRODUCTION	1
2 PSB-VVER TEST FACILITY	3
3 CL-4.1-03 EXPERIMENT	5
4 TRACE MODELS	7
5 STEADY STATE EVALUATION	15
6 QUALITATIVE ASSESSMENT OF THE SIMULATION RESULTS	17
7 QUANTITATIVE ASSESSMENT OF THE SIMULATION RESULTS.....	29
8 CONCLUSIONS	33
9 REFERENCES	35

LIST OF FIGURES

Figure 2-1	Design of the PSB-VVER Test Facility	3
Figure 3-1	Break Unit in Test 3 of PSB-VVER	5
Figure 4-1	RPV Nodalization	8
Figure 4-2	Pressurizer Nodalization.....	10
Figure 4-3	Loop #4 with the Break Unit	11
Figure 4-4	Hydroaccumulator Models.....	12
Figure 4-5	Radial Sectors in the Bottom Part of SG Model	13
Figure 4-6	Secondary Side Nodalization	13
Figure 6-1	Primary Pressure Evolution	21
Figure 6-2	Integral Break Mass Flow	21
Figure 6-3	Pressure Vessel Water Level	22
Figure 6-4	Pressure Differential in the UP	22
Figure 6-5	Pressure Differential in the Core Section.....	23
Figure 6-6	Loop Seal #1 Differential Pressure	23
Figure 6-7	Loop Seal #4 Differential Pressure	24
Figure 6-8	Cladding Temperature.....	24
Figure 6-9	Water Level of Hydroaccumulator #4.....	25
Figure 6-10	Water Level of Hydroaccumulator #2.....	25
Figure 6-11	Downcomer Coolant Temperature.....	26
Figure 6-12	Upper Plenum Coolant Temperature	26
Figure 6-13	Secondary Side Pressure in SG #4	27
Figure 6-14	Water Level in SG #4	27

LIST OF TABLES

Table 4-1	Nodalization Difference of the Models in the RPV Section.....	7
Table 5-1	Steady-State Parameters	15
Table 6-1	Sequence of the Main Events in the Transient	17
Table 7-1	Accuracy Categories for FFTBM-SM and SARBM.....	29
Table 7-2	FFTBM-SM and SARBM Results for the Selected Parameters.....	30

ACKNOWLEDGMENTS

We would like to acknowledge the helpfulness of Dr. Andrej Prošek (JSI, Ljubljana, Slovenia), who gave us access and instructions to the Microsoft Excel add-on developed for FFTBM-SM analyses.

The work presented in this paper involved the use of the TRACE thermal-hydraulic system code and the SNAP graphical user interface, both provided to the Institute under the CAMP agreement.

The research was partially funded by the Sustainable Development and Technologies National Programme of the Hungarian Academy of Sciences (FFT NP FTA).

ABBREVIATIONS AND ACRONYMS

AA	Average Amplitude
ADS	Atmospheric Steam Dump System
AF	Accuracy Factor
BDBA	Beyond Design Basis Accident
BME	Budapest University of Technology and Economics
CAMP	Code Application and Maintenance Program
CCFL	Countercurrent Flow Limitation
CL	Cold Leg
DAS	Data Acquisition System
DBA	Design Basis Accident
DC	Downcomer
DP	Differential Pressure/Pressure Differential
ECCS	Emergency Core Cooling System
EFW	Emergency Feed Water
EREC	Electrogorsk Research and Engineering Center on NPP Safety
FFCO	Friction Factor Correlation Option
FFT	Fast Fourier Transform
FFTBM-SM	Fast Fourier Transform Based Method with Signal Mirroring
FOM	Figure of Merit
FRS	Fuel Rod Simulator
FW	Feedwater
GUI	Graphical User Interface
HA	Hydroaccumulator
HL	Hot Leg
HPIS	High Pressure Injection System
HS	Heat Structure
HTC	Heat Transfer Coefficient
IAEA	International Atomic Energy Agency
ITF	Integral Test Facility
JSI	Jožef Stefan Institute
LOBI	LWR Off-Normal Behavior Investigation
LOCA	Loss of Coolant Accident
LP	Lower Plenum

LPIS	Low Pressure Injection System
MCP	Main Circulation Pump
NPP	Nuclear Power Plant
NTI	Institute of Nuclear Techniques
NUREG/IA	Nuclear Regulatory/International Agreement
PMK	Paksi Modell Kísérlet (in Hungarian)
PRISE	Primary-to-Secondary leakage
PRZ	Pressurizer
PSB-VVER	Primary System Benchmark for VVER
PV	Pressure Vessel
PWR	Pressurized Water Reactor
RELAP	Reactor Excursion and Leak Analysis Program
RPV	Reactor Pressure Vessel
SARBM	Stochastic Approximation Ratio Based Method
SBLOCA	Small-Break Loss of Coolant Accident
SG	Steam Generator
SNAP	Symbolic Nuclear Analysis Package
SPE	Standard Problem Exercise
SS	Steady State
TC	Thermocouples
TRACE	TRAC/RELAP Advanced Computational Engine
UH	Upper Head
UP	Upper Plenum
US NRC	United States Nuclear Regulatory Commission
VVER	Water-Water Energetic Reactor
WF	Weighting Factor(s)

1 INTRODUCTION

Hungary predominantly uses VVER-type pressurized water reactor technology for nuclear power generation; currently there are 4 units of VVER-440/V213 in operation at Paks NPP, with a proposed lifetime extension that would allow the units to continue operating beyond the 2030s. Moreover, due to the expected increase in electricity demand in the coming years/decades, the government decided to further increase the country's nuclear capacity. Part of this demand is planned to be met by two new VVER-1200 units, which are scheduled to be connected to the grid in the early 2030s. Therefore, our research focuses mainly on VVER technology.

In the last decades, considerable experience has been gained in the Budapest University of Technology and Economics, Institute of Nuclear Techniques (BME NTI) with thermal-hydraulic system codes. Besides the Finnish APROS code, recently we started using RELAP5 and TRACE codes, both provided to us by the US NRC in the framework of the CAMP agreement. First, two international IAEA benchmarks, performed on the PMK-2 small scale test facility, were analyzed simultaneously with the above-mentioned codes. As a result of this work, two NUREG/IA reports have been published [1] and [2]. In these studies, we thoroughly compared the best-estimate calculations with the benchmark data and to each other. Evaluations from qualitative and quantitative point of view pointed out several discrepancies between the models and calculations, based on which we drew some important conclusions for the future work.

In the current report, the large-scale ITF PSB-VVER (see Chapter 2) is under investigation, which also hosted several benchmark exercises, contributing to the VVER validation matrix [3]. One such experiment involved a SBLOCA in one of the cold legs, similarly to [1] and [2], so it was chosen as a reference to our calculations. In this paper, we summarize our results from three TRACE calculations performed with different nodalization approaches in the RPV section of the models. First, the description of the facility and the experiment analyzed is given, then, the simulation models and the modeling considerations are presented. Later, the steady-state and transient simulations are discussed, which is followed by a quantitative analysis of the results, performed with the well-known Fast Fourier Transform Based Method with Signal Mirroring (FFTBM-SM) [4]. Finally, the paper discusses the lessons learned and suggests possible ways to improve simulation accuracy in similar cases.

2 PSB-VVER TEST FACILITY

PSB-VVER served as a critical installation to study thermal-hydraulic processes and safety features of VVER-type reactors [3]. The integral test facility (ITF) is a scaled-down model of the primary and partly the secondary side of VVER-1000 (V320) units. It has been built in the late 90s at EREC (Electrogorsk Research and Engineering Center on NPP Safety) in Electrogorsk, Russia. During its operation, multiple experiments were conducted with the following objectives:

- assessment of the performance of safety systems used in the reference plant
- evaluation of the applied accident management strategies in design basis accidents (DBA) and beyond design basis accidents (BDBA)
- broaden VVER-related benchmarking experience with a possibility of system code validation
- investigation of scaling effects and other modeling aspects

Among similar test facilities, such as PACTEL, PMK-2 and ISB-VVER, PSB-VVER is considered rather as a large-scale test facility [5], as its dimensions are characterized by the volumetric scaling ratio of 1:300, compared to the reference plant. The electrical heating power of 10 MW is deposited to the core region by 168 power rods, which are arranged in the same hexagonal bundle as in VVER-1000. The reactor pressure vessel model is comprised of an external downcomer (DC), lower plenum (LP), core bypass (BP) and the main heated vessel. There is a connection moreover from DC top to upper plenum (UP) and upper head (UH) to CL#1, which prevents the formation of sections with non-moving coolant in steady state.

The secondary side model consists of vertically arranged steam generators with helical heat exchanger tubes and a common steam line which ends in a discharge tank called PSV-200. Feedwater (FW) is injected by separate FW pumps to the SGs through a ring-shaped dispenser at the top of the heat exchanger bundle. Moreover, pressure limitation is covered by the atmospheric steam dumping system (ADS) in the steam lines of the individual SGs.

The facility, as shown in Figure 2-1, models all 4 circulation loops so that the processes resulting in asymmetric loop behavior can be examined thoroughly. Aside from the piping and the MCP, one can find the SG collectors and 34 helical heat exchanger tubes in each loop. The pressurizer unit, by design, can be connected to loop #2 or #4 enabling the investigation of various configurations. Also, a number of break units have been installed for the investigation of LOCA-type accidents.

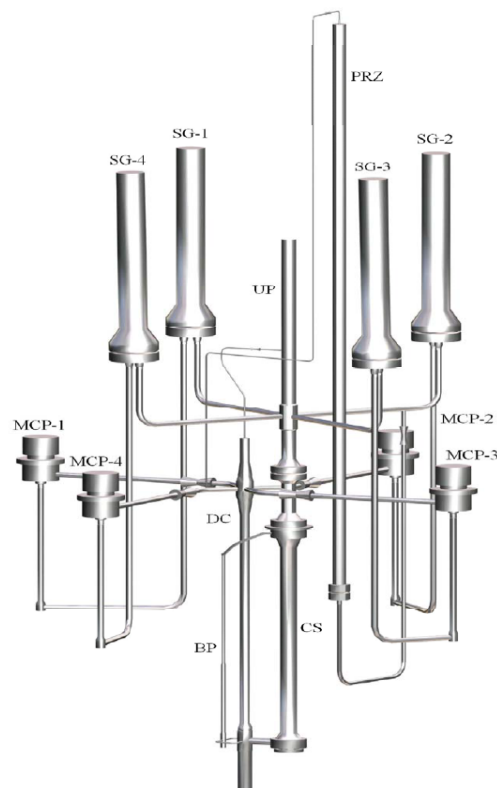


Figure 2-1 Design of the PSB-VVER Test Facility [6]

PSB-VVER is equipped with a range of safety systems, including emergency core cooling systems (ECCS). Four hydroaccumulator units (HA) serve as passive ECCS, connected to the DC and the UP in pairs. Active ECCS comprise both low- and high-pressure injection in the cold leg of loops #1, #3 and #4.

Experimental results were captured by the Data Acquisition System (DAS), which included over 1000 channels of different nature. Absolute and differential pressures were measured all along the primary side, water level measurements were made in the pressure vessel, PRZ, HAs and SGs, while coolant and wall temperatures (including those of the FRS) were determined at relevant positions. Other parameters, such as mass flows and velocities, coolant density, void fraction, pump speed and electric power were also used as reference during the calculations.

Thanks to the extensive design of PSB-VVER, the facility is capable of hosting various transient scenarios, including the full range of LOCAs, natural circulation and PRISE type accidents. One such test series has been organized by OECD [7] involving 5 predefined experiments, of which Test #3 has been chosen to assess our simulation data against.

Since one of objectives of CL-4.1-03 was to investigate the scaling effects of the facility, the experiment was designed to be as close as possible to the LOBI test scenario [8], which was similar in nature. Therefore, the initial FRS power was set to 11.5% of the scaled 10 MW and a cylindrical throttle was also installed in the break line in order to be in accordance with the design of LOBI. Furthermore, PRZ unit was connected to the broken loop (i.e., spray and surge line valves to loop #4 were open, while those to loop #2 were closed during steady state).

To mitigate the consequences of the accident scenario assumed in Test 3, the following safety measures were taken during the transient:

- termination of PRZ heaters and closing the spray valve
- valving off the UP heating line
- predefined decay power curve applied in core and core BP
- rapid MCP stop
- secondary side isolation
 - termination of FW pump operation
 - no EFW available
 - common main steam line valve closure
- ADS operation considered
- no HPIS is available
- available hydroaccumulator injection by HA-2 and HA-4 (both connected to the upper section of the DC)
- HA-1 & HA-3 (connected to the UP) are not in operation
- LPIS is available in loops #1, #3 and #4

4 TRACE MODELS

As mentioned in the previous chapters, the performance of 3 different TRACE models is to be investigated, among which the main differences lie in the used components and their nodalization in the RPV section. In the developed models, a distinction is made between the ones that use the built-in 3D Vessel component of TRACE for the most important parts of the RPV, and another model which only uses general Pipe components along the primary side. The other parts in the primary side, as well as the secondary side models are designed practically the same in order to better understand the reasons for potential discrepancies between the calculated data.

The models were built and set up in version 4.0.1 of the Symbolic Nuclear Analysis Package (SNAP) [9], which proved to be an effective graphical user interface (GUI) for model development in different codes, such as RELAP5 and TRACE. Simulations, performed with TRACE plug-in version of V5.0 Patch 6, were extracted in ASCII files and visualization of the obtained curves was done with MATLAB R2024b.

As mentioned, the 3 TRACE models have different nodalization details. In the first two, labeled as 'AZIM4' and 'AZIM1', 3D Vessel components are used to simulate the LP, DC and the main heated vessel (denoted as 'pressure vessel' or 'PV' hereafter) itself (see Figure 4-1). These models differ only in the azimuthal nodalization of the sections modeled with Vessel components (LP, DC, PV). While AZIM1 has no azimuthal sectors, in AZIM4 each axial plane is further refined into 4 azimuthal sectors of equal volume. This step is expected to allow the AZIM4 model to better capture the asymmetric processes taking place in the RPV. In both cases, number of axial layers in the LP, DC and PV models is 6, 19 and 51, respectively, while only one radial node is considered in each. Furthermore, in AZIM4 model, a number of VESSEL-VESSEL and PIPE-VESSEL connections had to be further subdivided to consider all azimuthal sectors. The model version consisting of only 'No accumulator' type Pipe components in the primary side (hereafter referred to as '*PIPE*') has a nodalization similar to that of AZIM1, although an extra axial cell needed to be added because of the positioning and connection of its outlet chamber. This is modeled as a concentric volume around the PV at the level of the HL junction (see [6] for the exact geometry). A summary of the model nodalizations is given in Table 4-1 below.

Table 4-1 Nodalization Difference of the Models in the RPV Section

	<i>AZIM4</i>	<i>AZIM1</i>	<i>PIPE</i>
Axial levels (PV)	50	50	51
Radial nodes (PV)	1	1	1
Azimuthal sectors (PV)	4	1	1
Axial levels (DC)	19	19	19
Radial nodes (DC)	1	1	1
Azimuthal sectors (DC)	4	1	1
Axial levels (LP)	6	6	6
Radial nodes (LP)	1	1	1
Azimuthal sectors (LP)	4	1	1

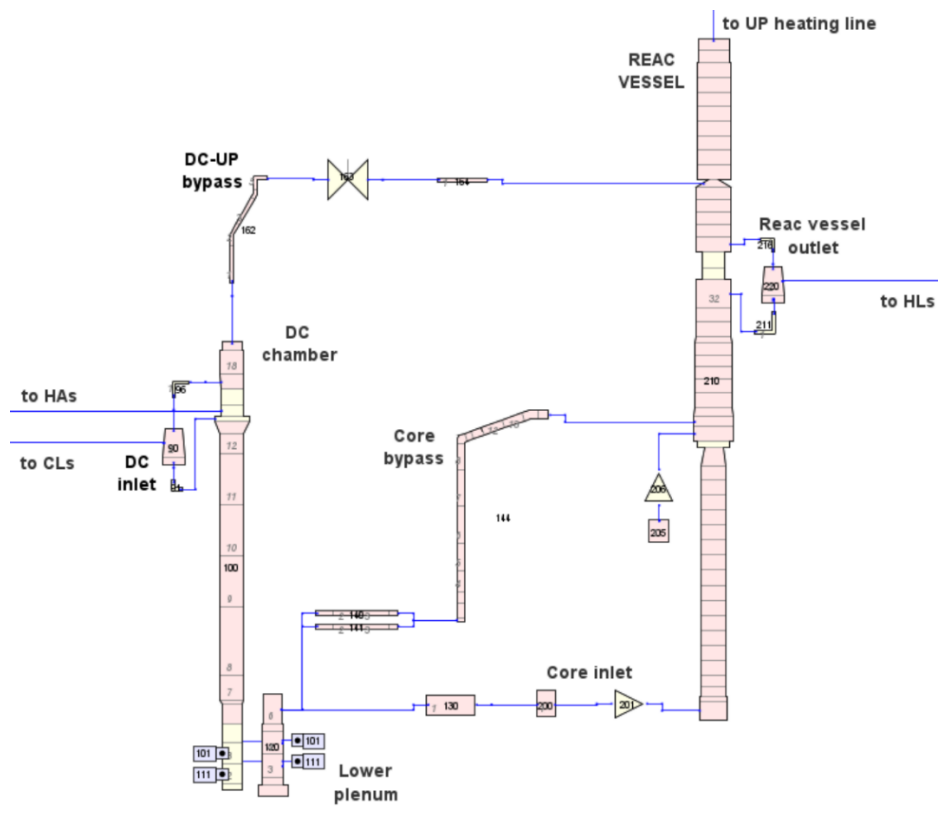
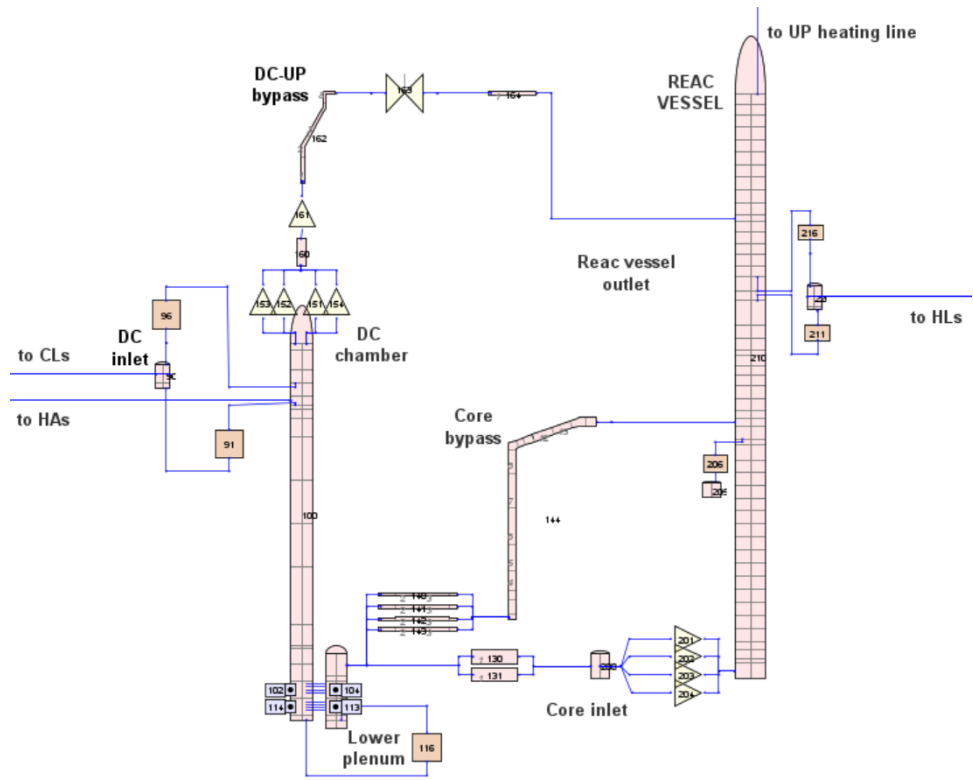


Figure 4-1 RPV Nodalization (Top: AZIM4, AZIM1; Bottom: PIPE)

FRS includes 29 heater rods equipped with thermocouples (TC) and 139 heater rods without TCs. The power is evenly distributed between the individual rods, however, the two categories required separate models, as their radial geometry is slightly different. Axially, 18 heat structure nodes represent the rods, of which 14 are heated and connected to the hydraulic nodes of 5-18 of the pressure vessel models. In the case of the model designated *AZIM4*, all 4 azimuthal sectors required an individual heater rod HS both for the ones equipped with thermocouples and those without. In addition, a relatively small proportion of the total power was deposited to the wall of the core BP section. Moreover, the heater rods required the definition of 3 new materials in TRACE: Periclase, Nichrome and the PSB-type Stainless Steel.

During the test, a partial core uncover is followed by a rewetting/reflooding period, so it is important to approximate the core water level as precisely as possible. Therefore, we decided to use the 'Level Tracking' option at the heated section (axial levels 4-20). However, in the case of the *PIPE* model, turning on this option caused unexpected behavior, resulting in frequent crashes and/or observably limiting the decrease of the pressure vessel collapsed water level. Hence, the Level Tracking option was turned off in this model.

In addition, appropriate CCFL models were applied at the upper bedplate even though there is no significant downward flow expected in the upper plenum.

The main differences between the models have been made in the RPV section, therefore the discussion in the following paragraphs applies to all 3 calculation models unless stated otherwise.

All 4 loops were explicitly modeled in TRACE, serving as an opportunity to capture those processes causing asymmetric loop behavior in the facility. In the pressurizer model (Figure 4-2), piping for both of the connection to loop #2 and #4 are present, although only the latter was actively involved in Test 3. The PRZ unit itself consists of 20 axial cells, the bottom 4 of which are equipped with heaters, maintaining the desired primary pressure in steady state (SS). Regarding the PRZ model, two modifications were made to speed up reaching SS conditions: a, the maximum heating power of the PRZ was increased from 80 kW to 400 kW, b, the correct PRZ level was set by an additional Fill component, controlled by a PI controller. These extra measures, however, did not affect the transient behavior, as the heating power at the end of SS was well below 80 kW (see Table 5-1) and the PRZ level control unit was terminated before commencing the transient.

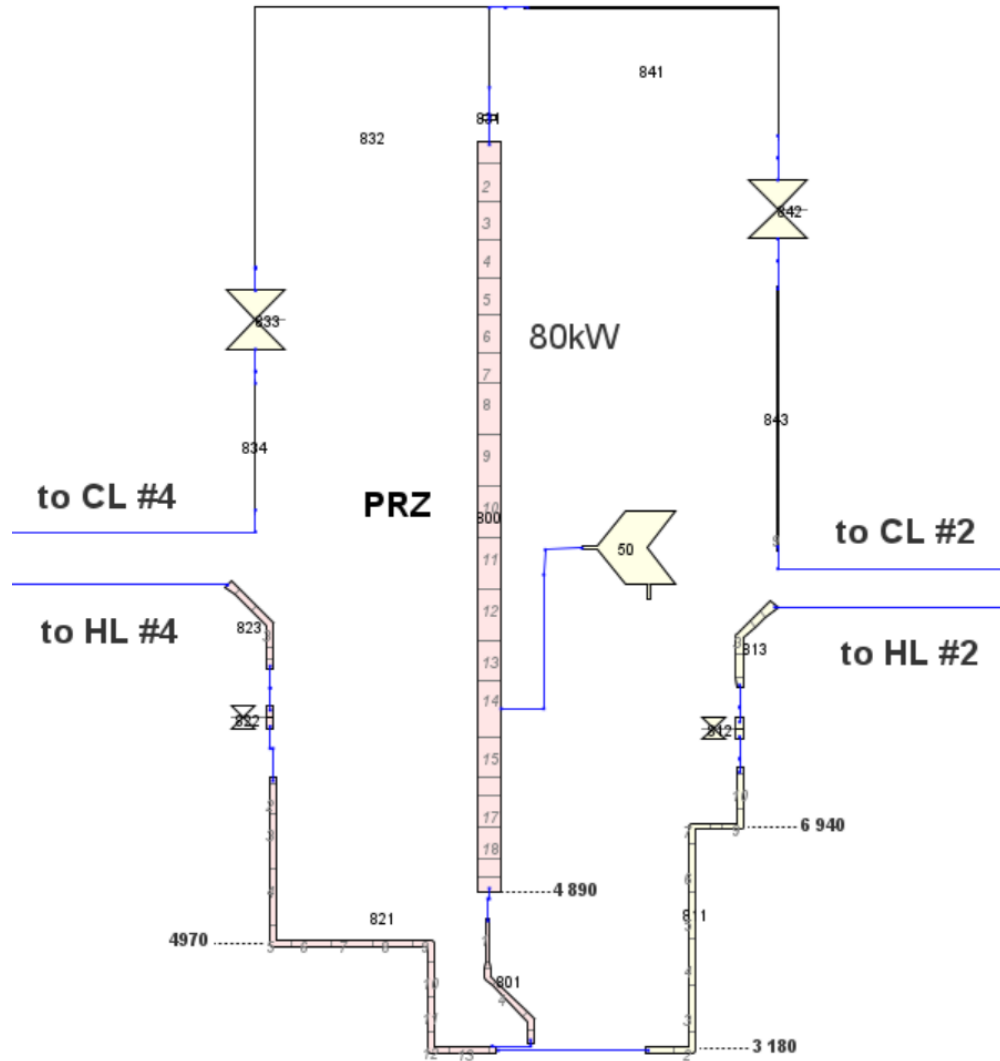


Figure 4-2 Pressurizer Nodalization

An extensive simulation model of the MCPs has been developed based on [10], which summarizes the necessary characteristics of TsNIS-1620 pump. Although the pump can handle two-phase flow for up to 1 hour, only single-phase characteristics are needed for this experiment, as the pump is stopped well before the formation of two-phase flow in the loops. In the models, therefore, Pump Type {1} was used by specifying single-phase head and torque curves, rated values and the appropriate friction factors. According to [6], an additional loop for cooling was used to remove the excess heat generated by the MCPs, however, due to the lack of information, neither this power nor the cooling circuit was modeled in TRACE.

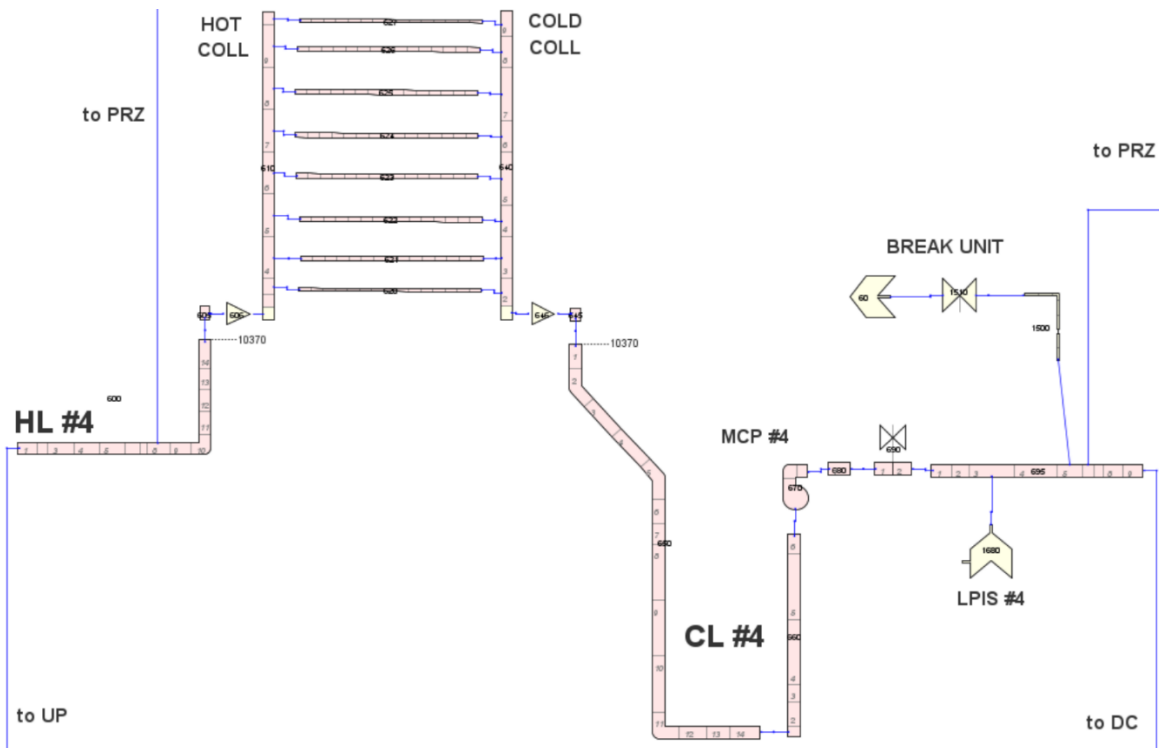


Figure 4-3 Loop #4 with the Break Unit

In case of the break unit, several nodalization settings were tested. At first, a detailed rupture model was developed for all 3 models with a geometry similar to that of the facility (Figure 3-1). Although the documentation was lacking some important data (e.g., width of catch tank #1, initial pressures in the tanks, boundary conditions), the gaps were filled with our best estimations. Nevertheless, during the model development we came to a conclusion, that a simple boundary-type break model (see break unit in Figure 4-3) gave practically the same results, so this simplification was eventually adopted to all TRACE models. At the narrowest point of the discharge line (top of the 10 mm constriction), the choked flow model was set with default multipliers and, following the TRACE user manual, Constant FRIC FFCO was applied. Hydroaccumulators considered in the current scenario, namely HA-2 and HA-4, are modeled with Accumulator Pipe Type {1} and are divided into 10 hydraulic cells. As shown in Figure 4-4, the walls of the HAs are taken into account, however, the heat transfer coefficients (HTC) of the outside surface in steady state have been set to zero in order to maintain the desired thermohydraulic conditions in the tanks. Heat losses along the HA connection lines are neglected.

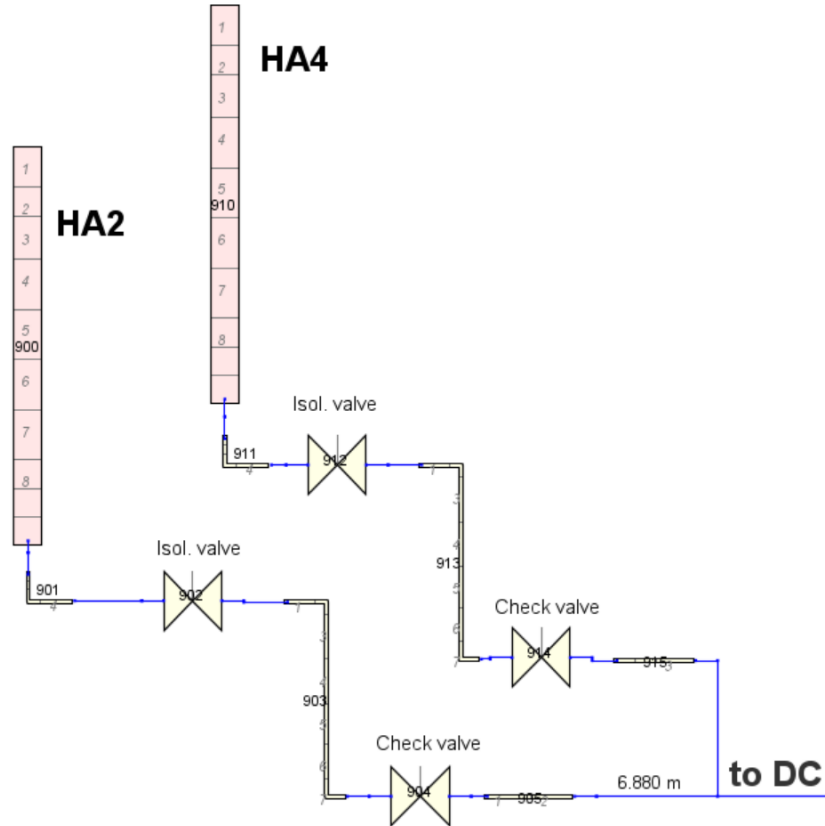


Figure 4-4 Hydroaccumulator Models

Heat transfer from the primary to the secondary side is provided by the steam generators. The flow area and the heat exchanging surface of the 34 heat exchanger tubes are modeled with 8 pipes, each divided into 15 nodes axially (Figure 4-3). As an inlet boundary to the secondary side, feedwater pumps are modeled with Fill components and the coolant enters the SG just above the top of the heat exchanger tubes, resulting in complex processes. Therefore, the steam generator unit (Figure 4-6) has been modeled with 3D Vessel components so that the lower part (containing the heat exchanger tubes) was radially split into two regions, as shown in Figure 4-5. This enabled the circulation of the secondary coolant in the SG. Axially, this section has 9 levels, while the upper part contains 3 axial layers with only one radial cell in each. The cells were not further divided azimuthally in the SG. In normal operational conditions, the generated steam passes the common main steam line and is discharged to the aforementioned condenser tank PSV-200. Unfortunately, no relevant data was found in the documentation regarding this unit, therefore it was modeled with a single boundary condition (Break component) in TRACE. On top of these, the individual ADS lines were built explicitly (see ADS #4 in Figure 4-6).

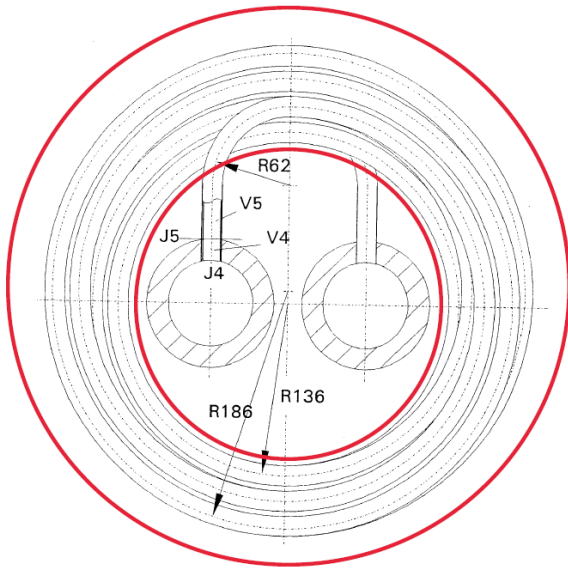


Figure 4-5 Radial Sectors in the Bottom Part of SG Model (Figure From [6] – Modified)

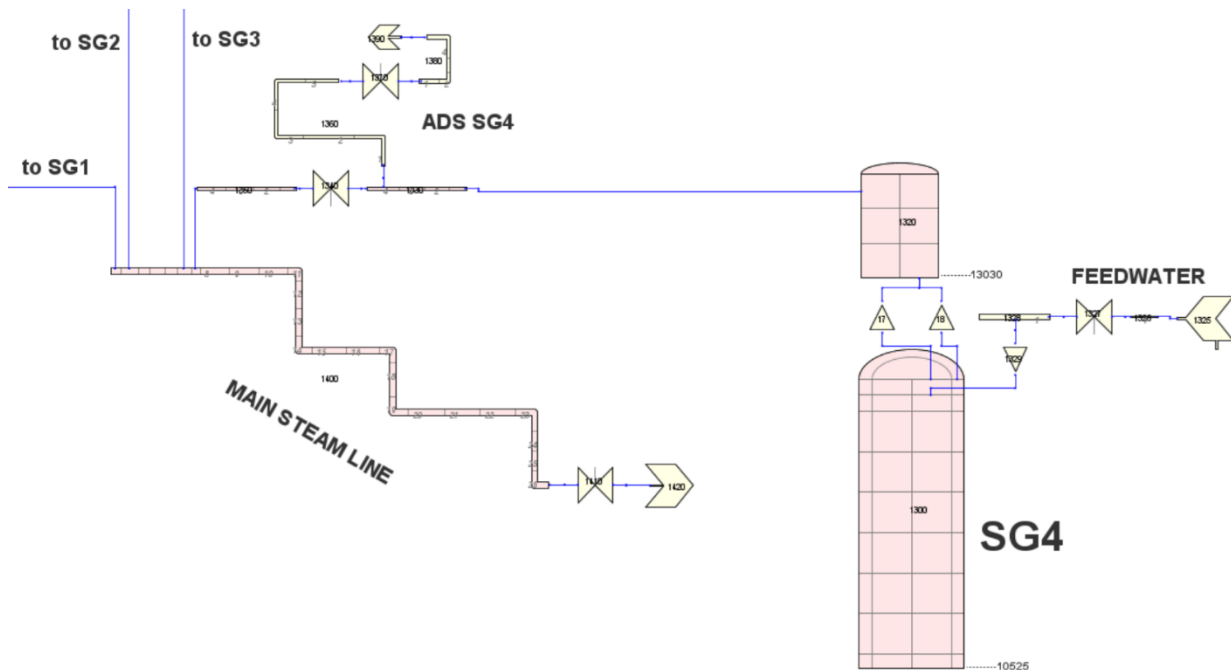


Figure 4-6 Secondary Side Nodalization

Extensive control systems were applied in accordance with the experiment documentation [6] to ensure proper SS conditions and accident response actions. As mentioned above, some modifications were made to the PRZ unit and the cooling circuit of the MCPs was not modeled. On top of that, the complete closure of the main steam line valve had been delayed in the models, as there was a non-negligible steam mass flow measured in MSL even after the documented valve closure timepoint. It may indicate an undetected leak or that the valve was not fully closed during the first 20 seconds of the transient.

5 STEADY STATE EVALUATION

Fidelity of transient calculations requires the establishment of proper steady-state conditions prior to the initiation of the scenario under investigation. For this purpose, a number of control systems were activated to set the desired thermohydraulic conditions in both the primary and secondary side. Pressure and heat loss distributions were set based on the measured pressure drops and heat losses across the facility ([11], [12]). In addition, both the geometry and fluid masses were checked, where sufficient data was provided in the documentation.

Table 5-1 Steady-State Parameters

Parameter	Meas. ID	Exp.	Accuracy	AZIM4	AZIM1	PIPE
Core outlet pressure, MPa	YC01P17	15.60	± 0.06	15.60	15.60	15.60
UP coolant temperature, °C	YC01T04b	311.6	± 4.2	312.6	312.2	312.4
DC coolant temperature, °C	YC01T259	282.6	± 3	284.9	284.8	284.8
Cladding temperature, °C (top, mid, bottom)	YC01T11	324.9	± 3	320.5	319.4	320.9
	YC01T84	309.1	± 3	308.7	307.4	309.8
	YC01T123	297.5	± 3	296.2	294.8	296.3
Loop mass flow rates, kg/s	YA01F01	1.97	± 0.1	1.96	1.98	1.96
	YA02F01	1.99	± 0.1	1.97	1.95	1.94
	YA03F01	1.99	± 0.1	1.96	1.95	1.94
	YA04F01	1.94	± 0.1	1.96	1.95	1.94
Power of fuel assembly, kW	YC01N01	1129	± 15	1130	1130	1130
Core bypass power, kW	YC01N02	14.9	± 0.7	14.9	14.9	14.9
PRZ heater power, kW	YP01N01	15.90	± 0.5	15.87	15.83	15.85
Coolant level in PRZ, m	YP01L02	3.05	± 0.3	3.05	3.05	3.05
DC diff. pressure, kPa	YC01DP01-05	-59.08	± 2.3	-58.00	-58.05	-58.04
Core diff. pressure, kPa	YC01DP07-10	-28.54	± 2.4	-30.11	-30.10	-30.01
UP diff. pressure, kPa	YC01DP11-15	-51.26	± 2.8	-50.93	-51.79	-51.93
Core BP diff. pressure, kPa	YC01DP17	-35.98	± 1.0	-36.82	-36.93	-36.97
SG pressures, MPa	YB01P01	6.88	± 0.05	6.88	6.88	6.88
	YB02P01	6.91	± 0.05	6.88	6.88	6.88
	YB03P01	6.93	± 0.05	6.88	6.88	6.88
	YB04P01	6.88	± 0.05	6.88	6.88	6.88
SG levels, m	YB01L01	1.90	± 0.08	1.90	1.90	1.90
	YB02L01	1.91	± 0.08	1.91	1.91	1.91
	YB03L01	1.94	± 0.08	1.94	1.94	1.94
	YB04L01	1.90	± 0.08	1.90	1.90	1.90
HA pressures, MPa	TH02P01	4.08	± 0.03	4.08	4.08	4.08
	TH04P01	4.07	± 0.03	4.08	4.08	4.08
HA levels, m	TH02L01	4.58	± 0.07	4.58	4.58	4.58
	TH04L01	4.57	± 0.07	4.60	4.60	4.60

As is can be seen in Table 5-1, almost all the important parameters defining SS conditions were within the uncertainty range of measured values. There is only one parameter, which is slightly outside these limits, namely, the temperature of the heater rods at their uppermost part. The reason of this observation is somewhat unclear to us, as an extensive FRS model was built with relatively fine nodalization, including all material regions specified in [6]. Furthermore, the FRS temperature below this point appears to be accurate and the coolant temperature increment along the heated section is also in a good agreement with that of the measurement. In the light of these findings, we would consider our models to be suitable for the transient evaluation of Test 3.

6 QUALITATIVE ASSESSMENT OF THE SIMULATION RESULTS

In this chapter, a comprehensive summary of our calculations is given. First, Table 6-1 lists main events that occur during the transient scenario. From this table, it is possible to compare the timing of these milestones predicted by the simulations with that determined in the experiment itself. Then, the prediction of several crucial parameters is shown and compared to each other and the measurement data in separate figures.

Table 6-1 Sequence of the Main Events in the Transient

Event	Measurement	AZIM 4	AZIM 1	PIPE
PRZ heater termination	-0.6	0.0	0.0	0.0
Break valve opening	0.0	0.0	0.0	0.0
Closing of the PRZ spray valve and UP heating line	0.0	0.0	0.0	0.0
SCRAM signal	4.1	8.5	8.4	8.9
MCP stop	8.0	9.7	9.5	10.1
PRZ emptied	10.0	9.7	10.4	10.8
FW injection termination				
SG #4	9.9	15.3	15.4	16.0
SG #1	11.5	17.0	16.8	17.4
SG #2	13.4	18.1	18.1	18.6
SG #3	17.5	19.0	19.0	19.6
MSL valve closure	17.5	30.9	30.9	31.6
ADS operation	33.5 – 95.4	30.1 – 82.0	29.5 – 88.7	30.3 – 86.5
SFE power reduction start	57.6	62.0	61.9	62.4
HA-4 injection	406 – 1365	392 - 1454	406 - 1518	409 - 1433
HA-2 injection	414 – 1452	398 - 1457	412 - 1520	416 - 1433
Core dry-out	2057	2026	2109	2252
LPIS injection onset	2432	2429	2539	2647
Transient termination	2593.4	3000	3000	3000

In the accident under investigation, one might define a few phases with different dynamics. As expected during a SB-LOCA scenario, a rapid blowdown takes place in the beginning, due to which the primary system quickly activates the SCRAM signal. The SCRAM signal triggers a number of actions, such as power reduction, stopping of the MCPs and secondary side isolation. In the simulations, the timing of the SCRAM signal is slightly delayed, which is the result of the different primary pressure evolution in the first 15 seconds of the transient (see Figure 6-1). However, this does not have a significant effect on the subsequent course of actions.

As seen, both the MCP stop and PRZ emptying time have been caught relatively well by all of the models. In the experiment, the FW flow rate was set by the valves downstream of the FW pump, however, in the models a different approach has been used, as the FW flow was adjusted directly by the pump model (Fill component). Although this modeling consideration proved to work well, the delayed SCRAM signal slightly postponed the FW injection time in each case. As mentioned earlier, an approximately 17 second time delay of the MSL valve closure has been introduced arbitrarily to the models, because of the non-negligible steam mass flow present in the main steam line even after the documented isolation time of the steam side (17.5 s).

Following the secondary side isolation, the ADS system limited the pressure of the SGs at 7.4 MPa. A few peaks have been observed in each case between around 30-90 s of the transient. Meanwhile, the power reduction on the SFEs has been initiated (with a 53.5 s delay to the SCRAM signal, as specified by the experimental description).

In the followings, no intervention is made by the control systems until the primary pressure decreases below 4.2 MPa, which is the onset of the HA injection. The load of the HAs is enough to supply the RPV system with fresh coolant for about 1000 s, the timing of which have been well caught by our TRACE models. In this phase, the depressurization of the primary side continues, although in a slower rate.

Terminating the passive ECCS injection, however results in a loss of primary coolant once again, which leads to the onset of the core dry-out approximately at 2050 seconds. This has been predicted at different times in the TRACE calculations (ranging between 2026 and 2252 seconds), with *AZIM4* model being the closest in this regard. When reaching the peak cladding temperature (PCT) of 500°C, LPIS starts to inject coolant with a temperature of 50°C to the cold leg of loops #1, #3 and #4. This proves to be sufficient to bring down the cladding temperatures and provide long-term cooling to the reactor model. Reaching relatively stable conditions terminates the experiment/simulations.

As seen in Table 6-1 and discussed above, all the important events and their timings were captured fairly accurately by the models, with a few (in some cases intentional) differences. In the followings, a more detailed insight is given into some of the key parameters by comparing the TRACE calculations to the experimental data.

Primary pressure (Figure 6-1) is one of the key parameters to describe the overall behavior of the facility. Following the initial steep pressure decrease, a short stagnation period occurs due to the intensive boiling taking place in the UP. The duration of this period is overestimated by the TRACE models, which indicates that less coolant could reach the break area compared to the experiment. This can also be observed in Figure 6-2, where the integrated break mass flow is shown. Until around 220 s, the discharged coolant is less than that indicated by the measurement. Worth mentioning that there is a rather unexpected behavior in the experiment at around 200 s, with a quick change in the trend of the discharge rate and heavy oscillations. This might be due to the complex break unit geometry, as this is the period, at around which the first catch tank fills up to the elevation of the outflow point, resulting in dynamic processes. During this time, all of our models underestimate the break mass flow, which could indicate some deficiencies in the modeling of the break unit (e.g., choked flow model). Unfortunately, TRACE only offers its built-in critical flow model where only choked flow multipliers are adjustable by the user. During the model development, we tried several break models (including detailed ones which comprise the whole discharge line and the tanks), however, similar results were achieved with only minor differences in each case. Therefore, it was decided to adopt the simplified break model (presented in Figure 4-3) with default multipliers. In our view, it would be, nevertheless,

worth investigating the root of this discrepancy. The developer might want to implement different models to the code (similarly to RELAP5 or APROS), between which the user could switch when needed. Note: A similar behavior was fixed in the APROS simulation of the same transient in [15] by appropriately choosing the critical flow model, for example.

As a result of the break mass flow underestimation, the water level in the pressure vessel (Figure 6-3) remained higher at this stage in all simulations. *AZIM4*, being the most detailed model in terms of RPV nodalization shows somewhat similar behavior to that of the measurement, yet still overestimating the water level. Although one might consider this as a rather minor improvement compared to *AZIM1* and *PIPE*, *AZIM4* is capable of catching the asymmetric loop behavior and the mixing processes in the RPV better, therefore, this is a clear example of the advantages of such a nodalization even in a scaled down facility of such magnitude.

Taking a look at the UP (see Figure 6-4) pressure differential, it is clearly visible, that some coolant remained temporarily trapped above the hot leg nozzles. In the facility, there is a constriction installed in this region, which could partially cause the issue, however, it has been modeled according to the experiment documentation. A significantly better performance of *AZIM4* (compared to the others) is observed, although still showing discrepancies to the measurement. Core differential pressure (Figure 6-5) simulations show a delay in the initial drainage of this section, while the following trends are well captured by the models, except *PIPE*, which predicted much less coolant in this section during the later stages of the transient. As a result of the higher inventory, loop seal drainages (Figure 6-6 and Figure 6-7) are also postponed in the early stages. It is worth noting here, that the formation of loop seals in the individual loops of the simulations was highly sensitive to the processes occurring in the system. Therefore, we refrain from drawing any conclusions regarding the differences in the permeability of the loops between the simulations and the experiment.

At around 450s, the water level decreases to a point, where its cooling potential is not enough to prevent a temporary increase in the cladding temperature (Figure 6-8). The core damage is prevented by the HA injection, which starts at around 410 seconds and is able to quickly rewet the core. In the simulations, the local minimum of the water level and its timing is seemingly predicted perfectly, however, it does not result in surge of cladding temperature in neither model. At this point, it has to be mentioned that setting the 3D level tracking option of TRACE did not affect the processes in the core region (and the upper plenum) in a substantial way, however, 1D level tracking caused unexpected behavior, seemingly 'flooring' the value at around 6 m, not allowing it to further decrease. Therefore, 1D level tracking was not used in the *PIPE* model. Furthermore, the processes in the RPV showed relatively low sensitivity to the axial nodalization of the core and UP region.

Hydroaccumulator injection characteristics were predicted with a good accuracy by all models (see Figure 6-9 and Figure 6-10), although in the beginning, *AZIM4* showed slightly more intensive injection rate than the other two due to the lower primary pressure at that time (Figure 6-1). The injection has been stopped on multiple occasions by the check valves, displaying short plateau-like characteristics. Due to the HA injection, the collapsed water level (Figure 6-3) has risen to around 6 m in the simulations (5.5 m in the experiment), which ensured the smooth depressurization of the primary pressure. Following the complete drainage of the HAs (at around 1450-1500s), however, the coolant level slowly started to decrease again up until the point, where the amount present in the core region was not sufficient to maintain the cooling effectiveness of the FRS. The timing of these processes was well captured by the simulations; however, the trends tend to be somewhat steeper than indicated by the measurements.

The main core dry-out has been initiated by the low water level, which, in the simulations required to be approximately 1 m below that of the measured value. Along with the absence of the first peak (at similar water levels between measurement and the calculations), this could indicate different coolant distribution and flow regime in the pressure vessel in TRACE, however, Figure 6-5 shows a good prediction of the core pressure differential in case of *AZIM4* and *AZIM1* models at the beginning of the core dry-out. This behavior of TRACE has been observed in our previous studies as well [13] [14], suggesting the requirement for deeper analysis (e.g., CHF model performances) of the issue. Apart from its timing, the main dry-out period has been well simulated by the models, as seen in Figure 6-8.

The processes on the secondary side commenced with a sharp pressure increase (Figure 6-13), resulting from the early isolation of the steam and feedwater sides. Reaching the ADS blowdown setpoint, depressurization valves open and closed multiple times until the primary pressure decreased to the level at which the direction of the heat transfer reversed. Following this, a rather slow, but steady depressurization of the secondary side took place, the trend of which was estimated well by the calculations. Due to the four steam generators being connected to each other by the common main steam line, their pressure evolution during the transient was practically the same, therefore, only one of them (namely, that of the SG4) is being presented here. Similar trends could be observed in SG water levels (Figure 6-14), where enough coolant remained to cover the top of the heat exchanger tubes during the whole experiment.

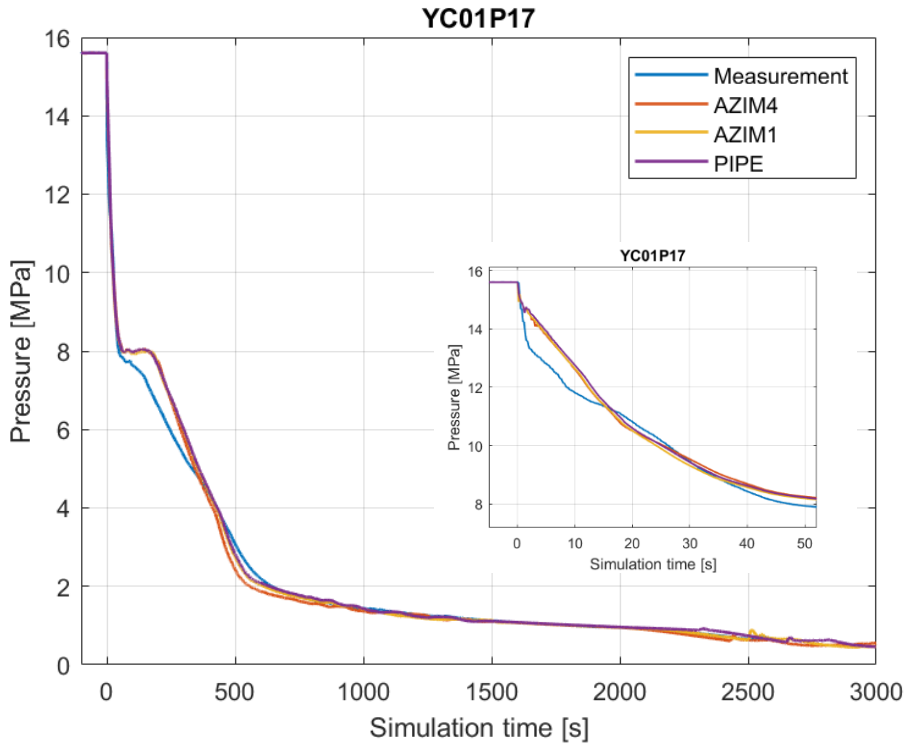


Figure 6-1 Primary Pressure Evolution

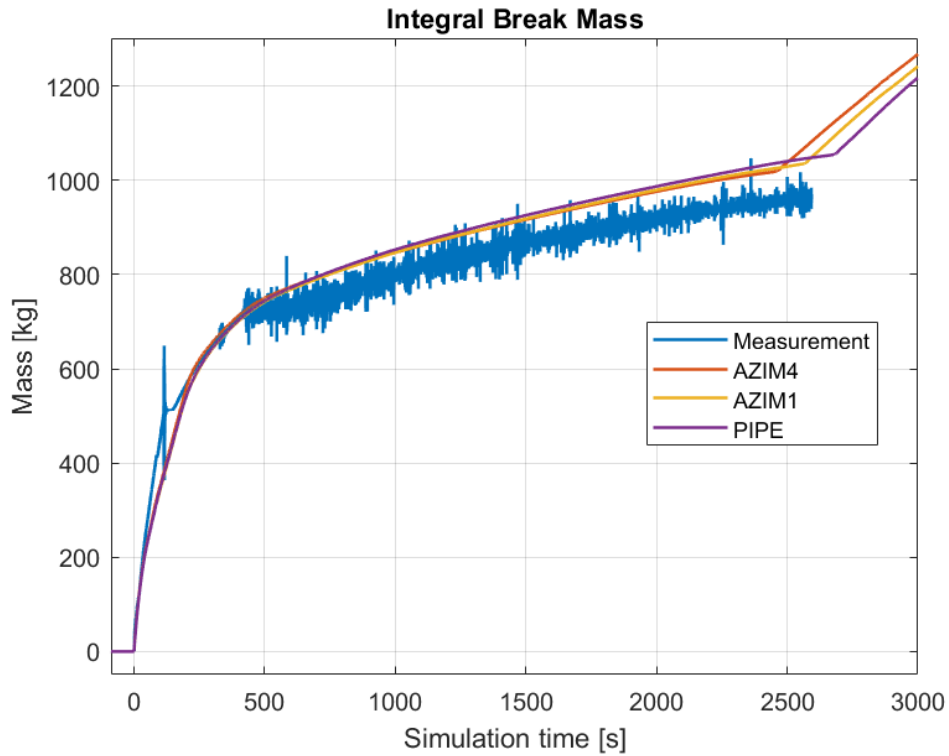


Figure 6-2 Integral Break Mass Flow

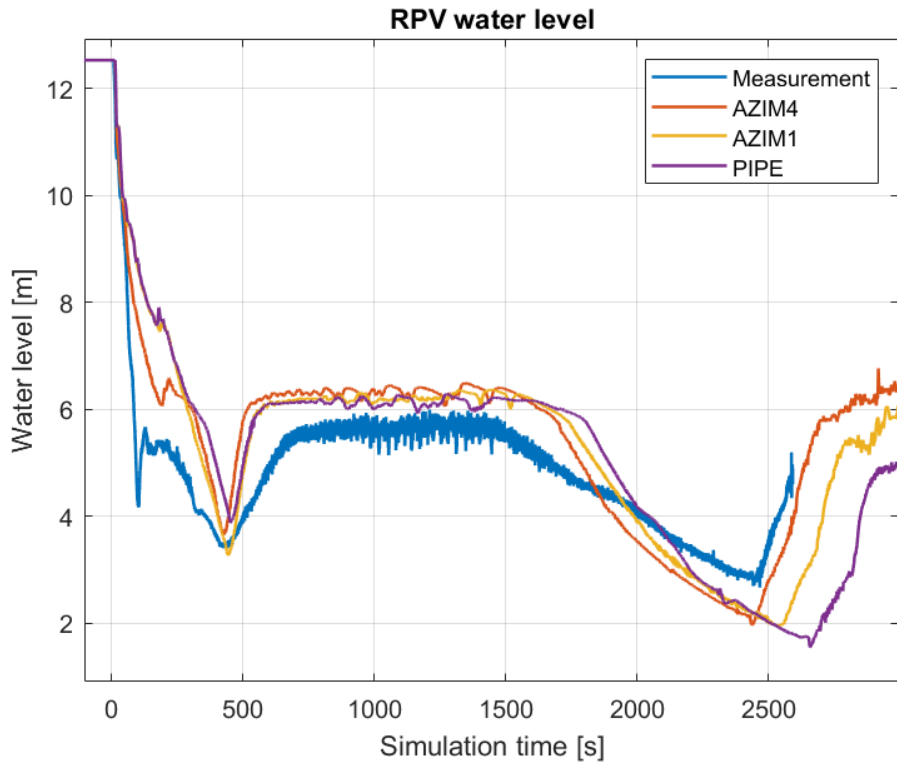


Figure 6-3 Pressure Vessel Water Level

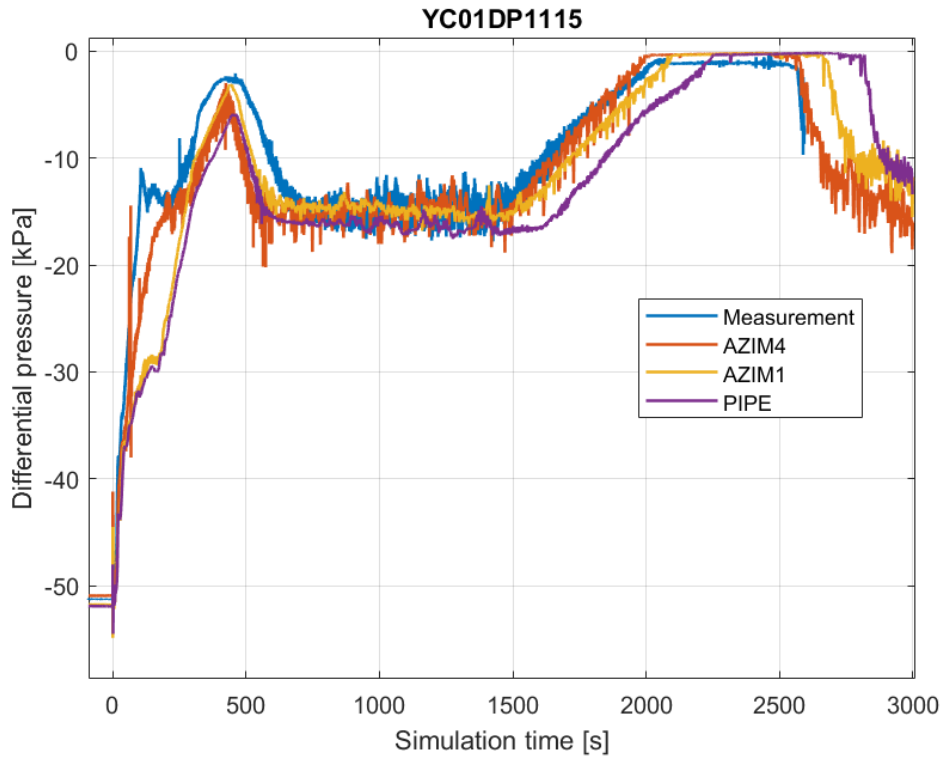


Figure 6-4 Pressure Differential in the UP

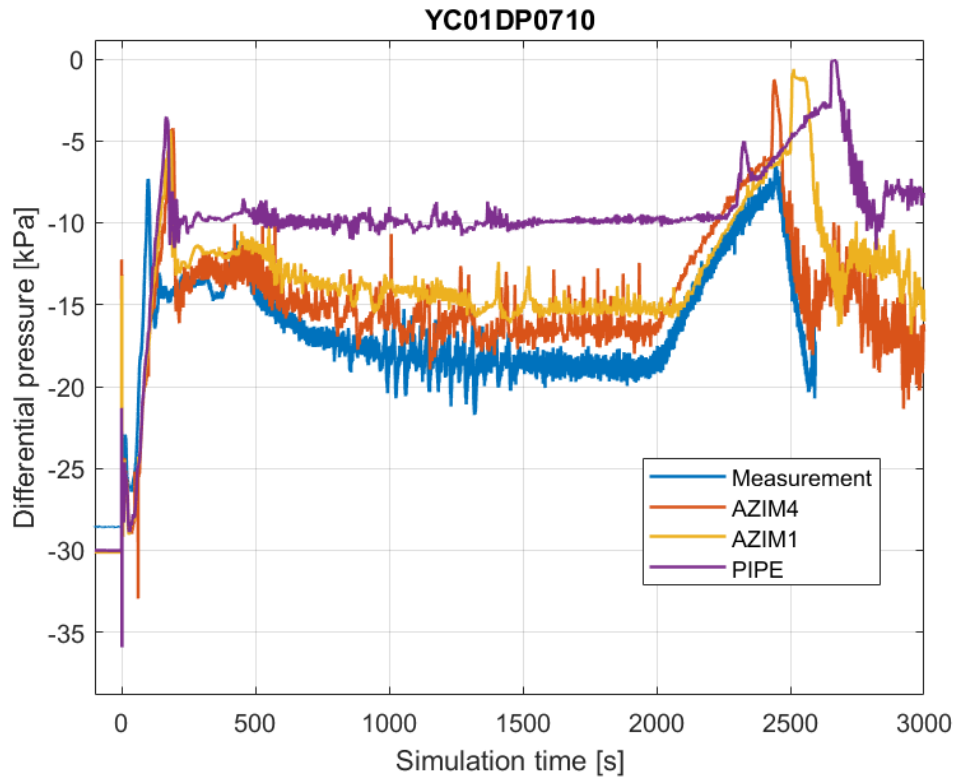


Figure 6-5 Pressure Differential in the Core Section

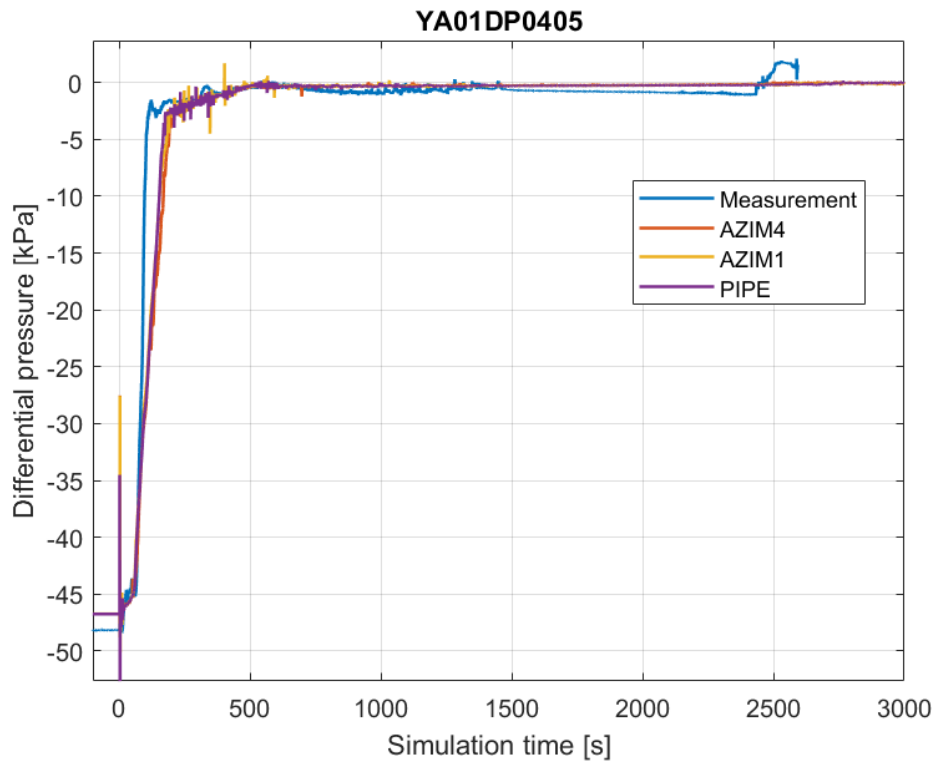


Figure 6-6 Loop Seal #1 Differential Pressure

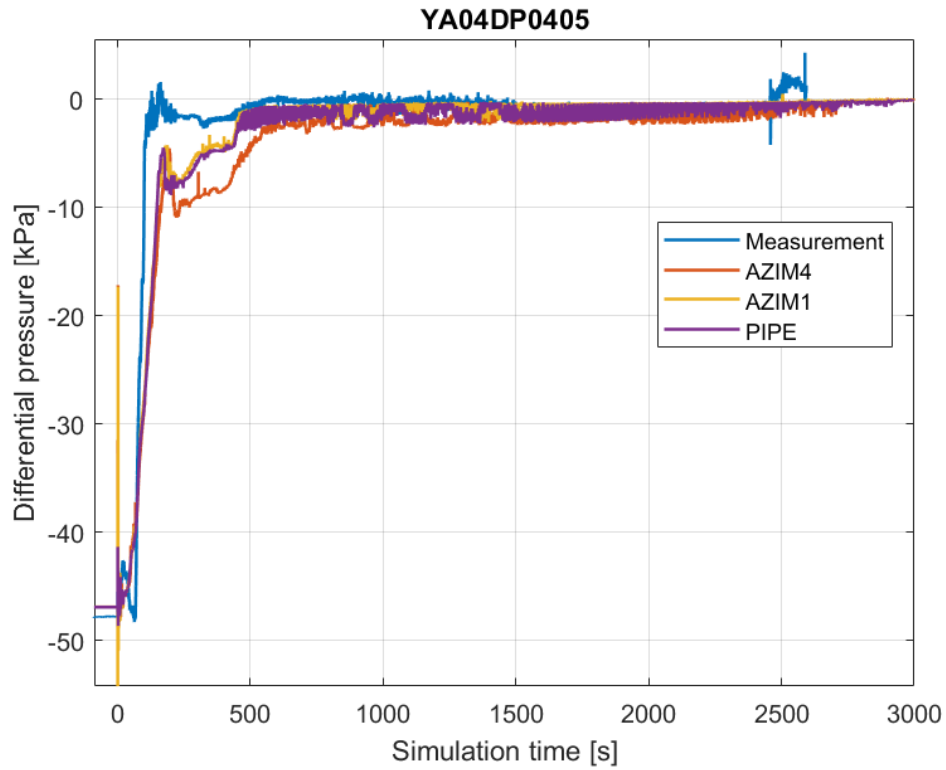


Figure 6-7 Loop Seal #4 Differential Pressure

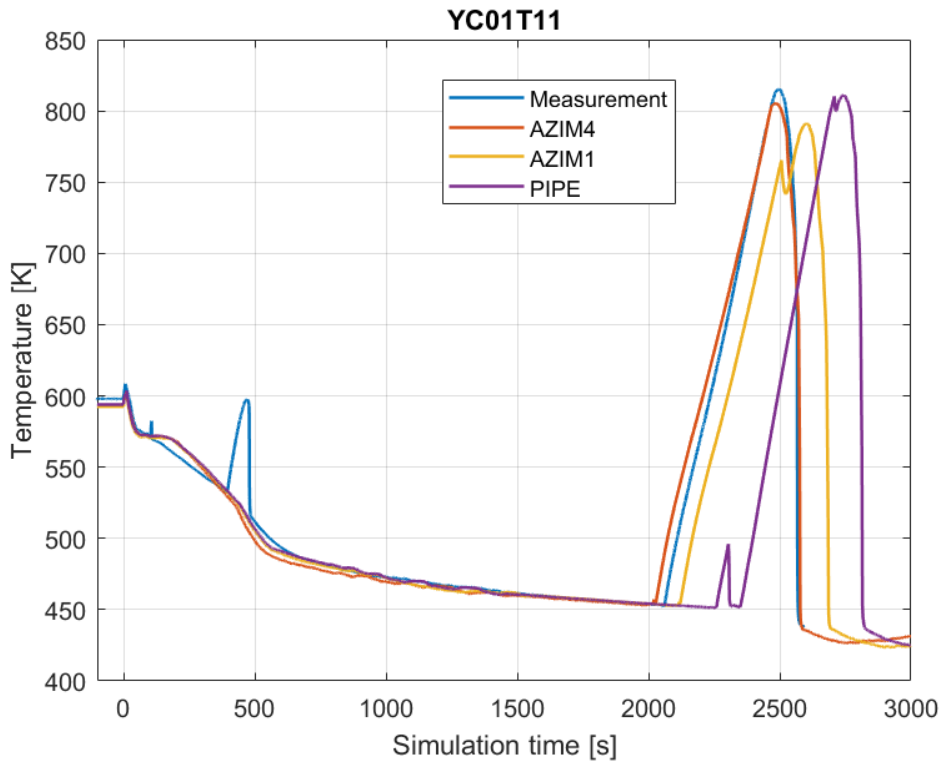


Figure 6-8 Cladding Temperature (Top of FRS)

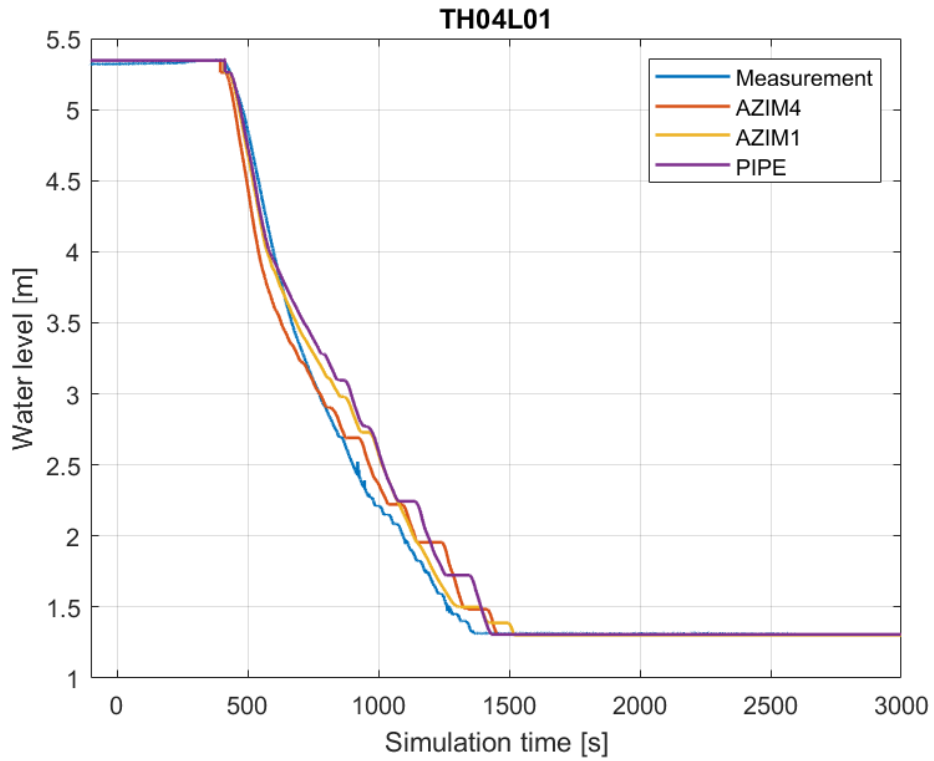


Figure 6-9 Water Level of Hydroaccumulator #4

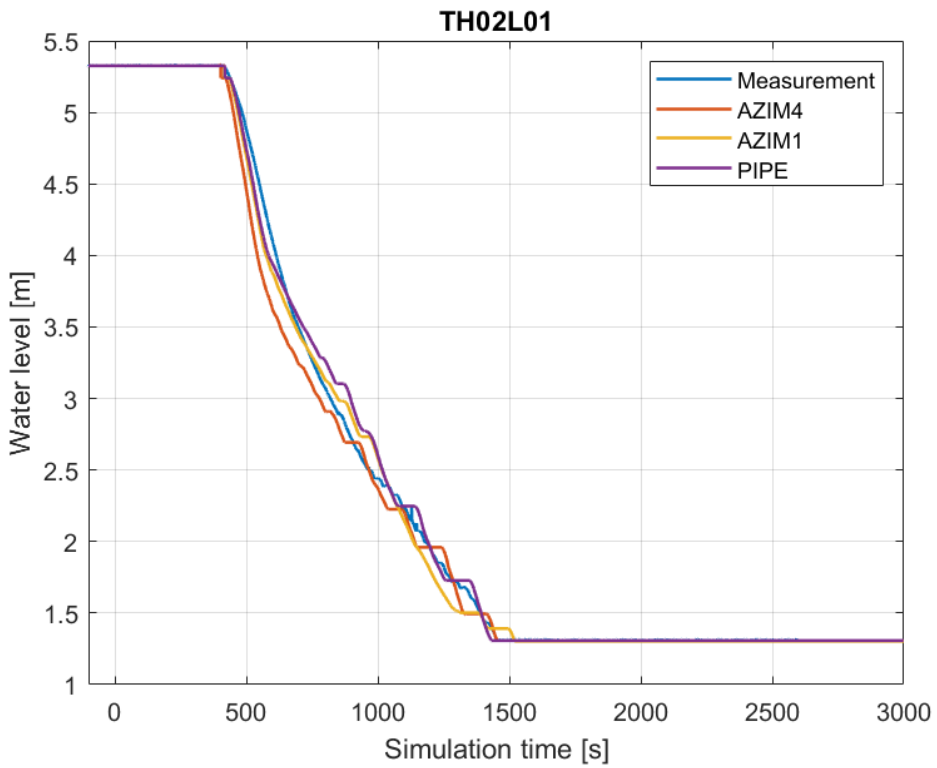


Figure 6-10 Water Level of Hydroaccumulator #2

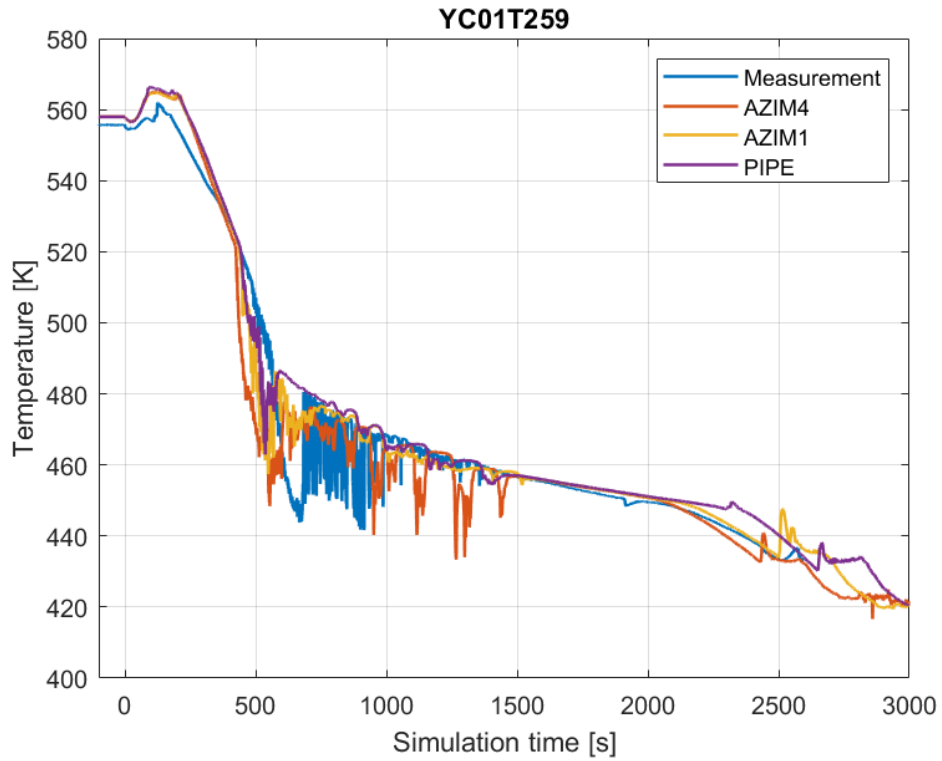


Figure 6-11 Downcomer Coolant Temperature

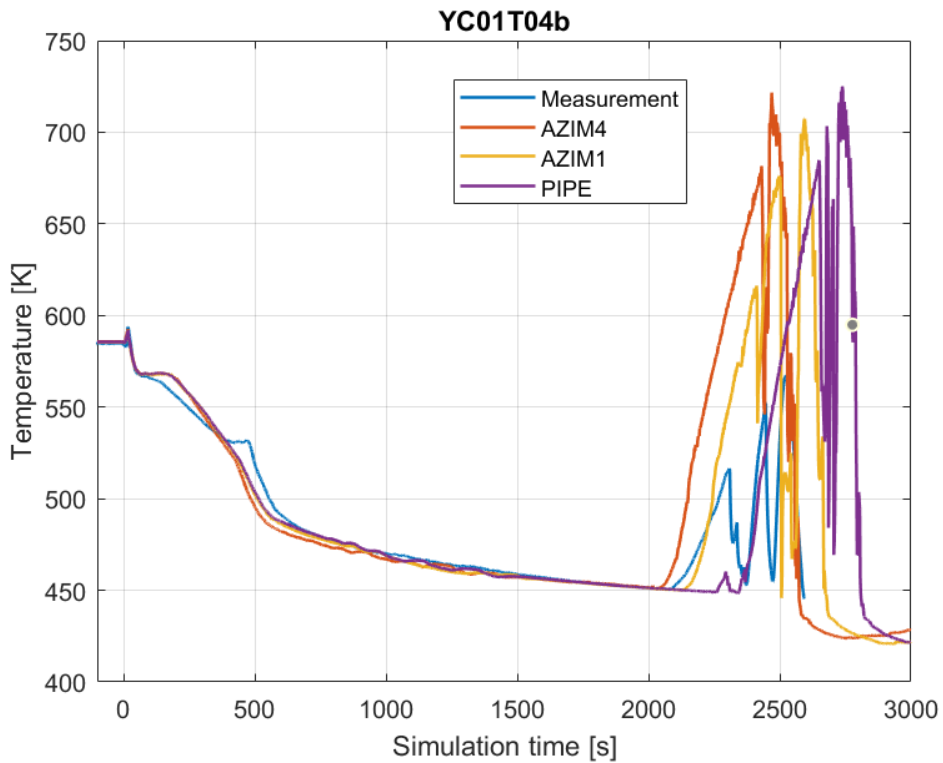


Figure 6-12 Upper Plenum Coolant Temperature

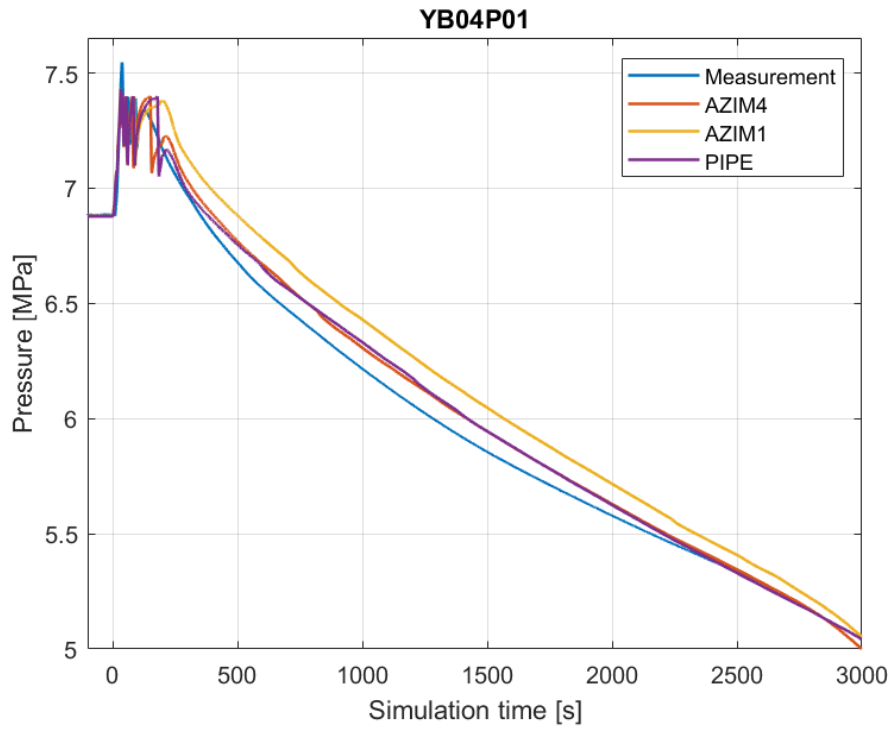


Figure 6-13 Secondary Side Pressure in SG #4

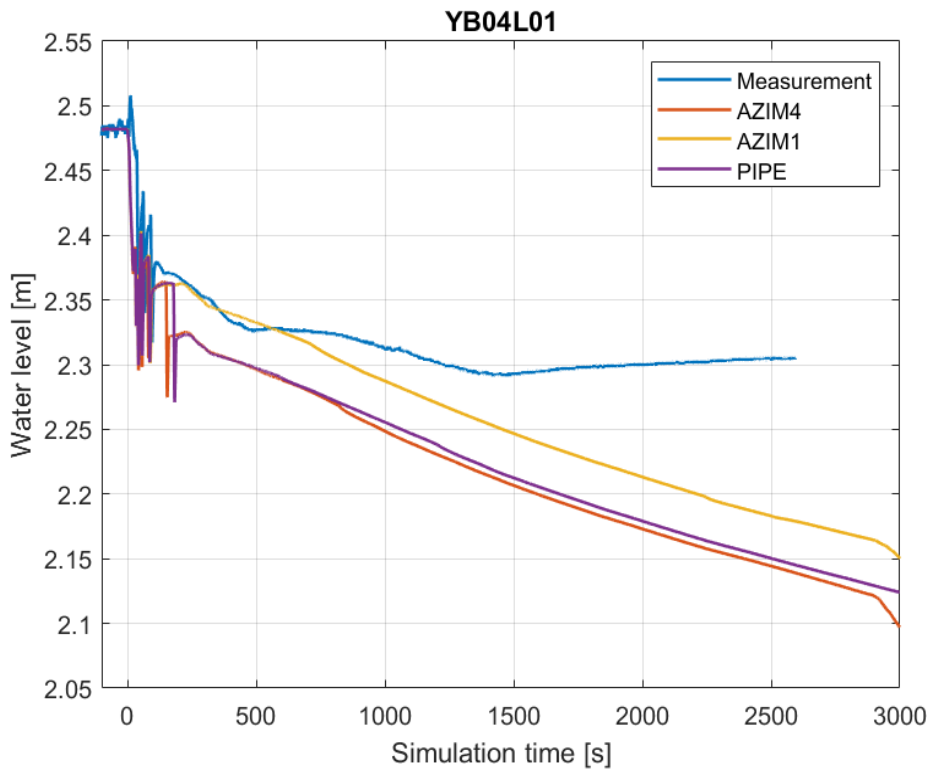


Figure 6-14 Water Level in SG #4

7 QUANTITATIVE ASSESSMENT OF THE SIMULATION RESULTS

In such benchmark exercises, where detailed measurement results are available, it is recommended to assess the performance of the constructed simulation models with quantitative tools as well. The two approaches complement each other well, since quantitative tools are capable of providing the user with a broad picture of the simulation accuracy in different stages of the transient under investigation. It is important however to be aware of their underlying principles and draw conclusions cautiously, taking into consideration the possible limitations of these methods. As we have recently gained significant experience using FFTBM-SM and SARBM methods in similar tests (such as in [13], [14] and [15]), both methods were adopted to assess our simulation results here.

FFTBM [16] is based on Fast Fourier Transform (FFT), which converts the data to the frequency domain. Comparing the calculation data to that of the reference (in this case experimental data) in the frequency domain results in the so-called Average Amplitude (AA_m), a simple value which increases as the simulation accuracy decreases. Throughout the years, the method has been improved several times resulting in the FFTBM-SM, which addresses the so-called edge effect of the original FFT based method [17] [18].

For the FFTBM-SM calculation, the user compiles a data set that represents the investigated experiment in an extensive manner. Then, proper weighting factors (WF) are to be specified to each parameter [19] depending on their nature. The input is processed by the method and the calculation results in the AA_m values for all the considered variables. Moreover, based on the WFs a total average amplitude ($AA_{m, tot}$) is obtained as a combination of the individual variables.

Stochastic Approximation Ratio Based Method (SARBM) is often used in conjunction with FFTBM-SM, as its Figure of Merit (FOM) is similar in behavior to that of the FFTBM [16]. The Accuracy Factor (AF), although in different ranges compared to the AA_m of FFTBM-SM, indicates those simulation results with a poorer accuracy with a higher value.

Table 7-1 lists the categories for the FFTBM-SM and SARBM, which can be used to assess the selected individual parameters, as well as the overall calculations. In both cases four categories are distinguished, namely, 'very good', 'good', 'poor' and 'very poor'. In addition, a general acceptability criterion has been introduced for the simulations ($K \leq 0.4$ for FFTBM-SM and $K \leq 0.2$ for SARBM).

Table 7-1 Accuracy Categories for FFTBM-SM and SARBM

Category	FFTBM(-SM)	SARBM
acceptable	$AA_m, AA_{m,tot} \leq K = 0.4$	$AF_{tot} \leq K = 0.2$
very good	$AA_m, AA_{m,tot} \leq 0.3$	$AF_{tot} \leq 0.1$
good	$0.3 < AA_m, AA_{m,tot} \leq 0.5$	$0.1 < AF_{tot} \leq 0.25$
poor	$0.5 < AA_m, AA_{m,tot} \leq 0.7$	$0.25 < AF_{tot} \leq 0.45$
very poor	$0.7 < AA_m, AA_{m,tot}$	$0.45 < AF_{tot}$

To emphasize its significance, a more stringent criterion of $AA_m < 0.1$ was established for the primary pressure in the original FFTBM. With the introduction of the improved version of the method (FFTBM-SM), the same criteria were maintained, although, the computed average amplitude values showed an increase, making it even more difficult to meet this requirement.

Therefore, drawing from the observations in our prior research [1] [2] [15], a K value of 0.2 has been suggested and used here for the primary pressure.

For the calculations, an extensive list of parameters has been compiled. Altogether 31 different parameters (Table 7-2) were chosen to best describe all the relevant processes taking place in the primary and secondary side. For the exact location of the measurement gauges the reader is advised to refer to [6]. In Table 7-2, the goodness of FOM values for FFTBM-SM and SARBM are categorized for each parameter according to Table 7-1. Dark green represents 'very good', light green 'good', light brown 'poor' and red 'very poor' accuracy, as indicated in Table 7-1.

Table 7-2 FFTBM-SM and SARBM Results for the Selected Parameters

Parameter	FFTBM-SM (AA_m , $AA_{m,tot}$)			SARBM (AF , AF_{tot})		
	AZIM4	AZIM1	PIPE	AZIM4	AZIM1	PIPE
YC01P17	0.198	0.198	0.196	0.084	0.077	0.078
YP01P01	0.149	0.143	0.137	0.084	0.077	0.079
YB01P01	0.138	0.152	0.132	0.014	0.028	0.014
YB04P01	0.123	0.140	0.115	0.013	0.027	0.013
YB01L01	0.142	0.136	0.143	0.014	0.018	0.013
YB04L01	0.180	0.164	0.178	0.042	0.028	0.039
TH02L01	0.201	0.134	0.148	0.059	0.037	0.035
TH04L01	0.187	0.165	0.200	0.061	0.054	0.072
YC01T11	0.334	0.506	0.663	0.034	0.080	0.151
YC01T84	0.150	0.485	0.384	0.010	0.068	0.048
YC01T123	0.087	0.082	0.080	0.008	0.007	0.009
YC01T259	0.320	0.282	0.281	0.022	0.017	0.019
YC01T04b	0.836	0.870	0.361	0.101	0.082	0.050
YC01N01	0.091	0.091	0.098	0.019	0.018	0.021
YA01T04	0.352	0.500	0.345	0.055	0.046	0.041
YA01T25	0.165	0.164	0.139	0.014	0.014	0.013
YA04T04	0.437	0.513	0.412	0.065	0.046	0.043
YA04T25	0.166	0.170	0.161	0.016	0.022	0.019
YC01DP0105	0.497	0.599	0.644	0.089	0.135	0.181
YC01DP0710	0.868	0.882	0.928	0.159	0.257	0.458
YC01DP1115	0.658	0.644	0.654	0.199	0.281	0.336
YC01DP17	0.820	0.859	0.934	0.204	0.303	0.437
YA01DP0405	0.684	0.616	0.707	0.408	0.326	0.342
YA01DP13	0.388	0.345	0.365	0.227	0.203	0.213
YA01DP14	0.439	0.477	0.402	0.290	0.280	0.275
YA04DP0405	0.668	0.623	0.632	0.399	0.317	0.334
YA04DP13	0.428	0.381	0.541	0.239	0.217	0.219
YA04DP14	0.696	0.729	0.680	0.357	0.361	0.352
Int. break mass flow	0.377	0.376	0.380	0.063	0.064	0.070
PV water level	0.503	0.572	0.574	0.164	0.187	0.197
Prim. mass	0.445	0.451	0.459	0.230	0.227	0.249
Total	0.328	0.368	0.319	0.074	0.077	0.083

As seen in the table above, the accuracy of most parameters falls under the 'very good' and 'good' categories, including that of the primary pressure (YC01P17) and the overall simulation (Total). Therefore, the focus will be on the worse performances in the followings.

FFTBM-SM points out the top cladding temperature (YC01T11) as the first such parameter in *AZIM1* and *PIPE* models. As discussed before, the cladding temperatures are mostly driven by the saturation temperatures in the core section. This trend is simulated well by the codes. The discrepancies indicated by FFTBM-SM stem rather from the two dry-out stages. The first, short core uncover (Figure 6-8) has not been captured by neither of the models, although the pressure vessel water levels are in a good agreement with the measurements at that time. However, the larger part of the discrepancy comes from the second, main peak. Although its shape and timing are well captured (especially in *AZIM4* and *AZIM1*), FFTBM tends to be overly sensitive to the timing of such rapid changes, meaning that in some cases a relatively small shift between the calculation and the reference is evaluated as a significant discrepancy. Hence, the elevated AA_m values here are attributed to the intrinsic behavior of the method.

'Very poor' results were obtained in case of the upper plenum coolant temperature (YC01T04b) of *AZIM4* and *AZIM1* models, while that of the *PIPE* model showed surprisingly good accuracy in FFTBM. As seen on Figure 6-12, each model significantly overestimates the mixture temperature once the core dry-out starts. Although the trends are similar (2-3 peaks separated by quick temperature drops), the magnitude is much higher in the simulations. Its timing follows the initiation of the main core dry-out, *AZIM4* and *AZIM1* being much closer (compared to *PIPE*) to the experiment in this regard. In spite of this, the accuracy of *PIPE* is significantly better, which is attributed to the delay of the dry-out phase, as discussed below. On the one hand, the trend and timing of the first temperature peak of *PIPE* match those of the second peak of the measurement, practically resulting in an overlap over an extended period. On the other hand, simulation data beyond ~2600 s is not included in the quantitative evaluation, as measurement data is only available up to 2592 s. Consequently, a significant portion of the dry-out peaks does not contribute to the average accuracy of the parameter. This effect is also present in *AZIM1*, although to a much lesser extent. Due to these factors, FFTBM produces misleading results for *PIPE*, which should be interpreted with caution. This case further highlights the methods' sensitivity to delayed signals.

In case of the RPV (YC01DP0105, YC01DP0710, YC01DP1115, YC01DP17) and loop differential pressures (YA01DP0405, YA04DP0405, YA04DP14), most of the inaccuracy is accumulated by the delayed drainage of the given section, which can be seen in the figures of the previous chapter. Simulation accuracies along the heated section (YC01DP0710 – Figure 6-5) are evaluated somewhat similar by FFTBM. In our view, however, both *AZIM4* and *AZIM1* outperform *PIPE* in the later stages of the transient (i.e., after the initial drainage of the section), as *PIPE* model predicts significantly lower pressure drop/water level in this section. The explanation for this behavior was given by comparing the time dependent AA -s of the parameter, which showed, that *PIPE*'s timing of the initial drainage is superior to the other two models. Although, this rather minor difference is overvalued by FFTBM. Also, the evolution of the upper plenum DP is best approximated by *AZIM4* (Figure 6-4), which is not shown by FFTBM. The reason behind this most likely stems from the oscillations observed in *AZIM4*, which contributed to the higher AA_m -s of the model. Similarly, the accuracy of the hot and cold collectors and the CL loop seal (Figure 6-6, Figure 6-7) simulations are mostly affected by the delay of their initial drainage.

On the other hand, SARBM tends to be less sensitive to the shift in signals and to the oscillations, as seen on the AF values of the top cladding temperature, UP coolant temperature and the pressure differentials, for example. While none of the parameters was put into the 'very poor' category, generally the pressure differentials were evaluated as the least accurate, similarly to FFTBM. Assessment of SARBM on the individual parameters, as well as the total accuracies is mostly in line with our conclusions based on Chapter 6, (i.e., model *AZIM4* produces the most and *PIPE* produces the least accurate results in the current experiment. Nonetheless, the differences are rather minor, and each model is suitable for the test).

To summarize the chapter, acceptability criteria of the FFTBM-SM and SARBM methods are met in each case (note: as suggested earlier, primary pressure criterion of $K < 0.2$ was considered here). Generally, SARBM assessed the models as 'very good', showing only minor differences between them, which results in a ranking as follows: *AZIM4* > *AZIM1* > *PIPE*. According to FFTBM-SM, all model versions were evaluated as 'good', but a different order was determined based on their accuracies, where *PIPE* version was considered as the most suitable (*PIPE* > *AZIM4* > *AZIM1*). This, however, is presumably due to the underlying principles of the methodology, by which some types of signal discrepancies are magnified to a level, which affects the overall assessment of the simulations, possibly resulting in misleading results. It is therefore essential in similar studies to integrate both qualitative and quantitative approaches, as the two complement each other.

8 CONCLUSIONS

PSB-VVER is a large-scale model of the VVER-1000 (V320) units. Due to its extensive design, the facility proved to be an invaluable member of those installations, which helped to gather benchmark data for VVER-type reactors. In this paper, we have assessed the performance of our TRACE models with different nodalizations in the RPV section.

First, an overview of the facility is given, which is followed by the specification of the experiment (CL-4.1-03) under investigation. Then, a detailed description of the TRACE models, along with the relevant modeling considerations is presented. The simulation results are evaluated first on a qualitative basis, which is complemented with a quantitative assessment, performed with FFTBM-SM and SARBM methods.

In the SB-LOCA scenario, the injection of 2 passive hydroaccumulators and the LPIS in 3 of the 4 loops is considered. During the transient, the loss of primary coolant and the temporary uncovering of the heater rods was successfully handled by the ECCS before reaching a stable state with sufficient long-term cooling for the core.

In our Institution, three TRACE models were constructed with different nodalization approach in certain parts of the RPV. Two of the models utilized the 3D Vessel component of TRACE, while in the third one, the primary side comprised of only Pipe components.

In general, it can be concluded, that all 3 models were in a good agreement with the measurements from the qualitative point of view, as the processes with significant importance and their timings were caught well. However, a few notable discrepancies were spotted, such as the underestimation of the break flow of the calculations in the initial phases of the transients. Because of this, higher RPV water levels were predicted during this stage. Although a similar local minimum of the collapsed water level was achieved in the simulations as that of the experiment, the occurrence of the first peak of the cladding temperature was not observed in neither of them. Also, lower water levels were present in TRACE at the start of the main core dry-out, which aligns with our previous observations. These findings would require further investigation, possibly involving the assistance from the developers of the code.

In the quantitative assessment, all calculations fulfilled the acceptability criterion of both methods. Moreover, SARBM indicates that the TRACE simulations are 'very good', as the total accuracy factor is well below the value of 0.1. Nevertheless, the methods pointed out several parameters, in which notable discrepancies can be observed compared to the measurement. FFTBM-SM evaluated the pressure differentials of the pressure vessel, hot & cold SG collectors and the upper plenum mixture temperature as the ones with the least accuracy. On the other hand, SARBM indicates better results in general, highlighting only the pressure drop inaccuracies.

FFTBM-SM suggested ($AA_{m,tot}$) *PIPE* model as the closest to the experiment, although some artefacts of the method influenced this result. Therefore, we evaluated *AZIM4* with a better overall performance. SARBM supported our observations, indicating only small differences between the models, with a ranking of *AZIM4* > *AZIM1* > *PIPE*.

With the combination of the two approaches (Chapter 6 and 7) the problematic areas were recognized, based on which the models could be further refined in the future. Also, the importance of the critical interpretation of the result given by the used quantitative models was highlighted.

In addition, a few aspects of the sensitivity of the models were covered indicating the significance of the CCFL model at the upper bedplate, and the level tracking option. Areas with less impact on the overall simulations included the modeling of the break unit and the axial nodalization of the RPV.

9 REFERENCES

- [1] Orosz, R., Varju, T., Aranyosy, Á., Holl, V., Hajas, T. & Aszódi, A., 2022. RELAP5, TRACE and APROS Model Benchmark for the IAEA SPE-4 Experiment. International Agreement Report (NUREG/IA-0533)
- [2] Orosz, R., Varju, T., Aranyosy, Á., Holl, V., Hajas, T. & Aszódi, A., 2023. RELAP5, TRACE and APROS Model Benchmark for the IAEA SPE-2 Experiment. International Agreement Report (NUREG/IA-0544)
- [3] OECD NEA, 2001. Validation Matrix for the Assessment of Thermal-hydraulic Codes for VVER LOCA and Transients NEA/CSNI/R(2001)4
- [4] Prošek, A., Mavko, B., 2009. Quantitative Code Assessment with Fast Fourier Transform Based Method Improved by Signal Mirroring. International Agreement Report (NUREG/IA-0220)
- [5] Kral, P., 2007. Experimental facilities for VVER thermal hydraulic research and code validation (COVERS). Int. J. Nuclear Energy Sci. Technol. (IJNEST) 3 (3)
- [6] Melikhov, O.I., Elkin, I.V., Lipatov, I.A., Dremin, G.I., Nikonov, S.M., Kapustin, A.V., Rovnov, A.A., Gudkov, V.I., Antonova, A.I., 2004. Standard Problem Definition Report (Test 3), OECD PSB-VVER REPORT No. PSB-21.
- [7] Melikhov, O.I., Elkin, I.V., Nikonov, S.M., Basov, A.V., Kapustin, A.V., 2008. Final Report, OECD PSB-VVER Project (Version 4), PSB-VVER REPORT No. PSB-32
- [8] D'Auria, F., Galassi, G.M., 1992. Use of LOBI data for scaling of thermalhydraulic phenomena, LOBI seminar, Arona, Italy.
- [9] Jones, K., Rothe, J., Dunsford, W., 2009. Symbolic Nuclear Analysis Package (SNAP), Common Application Framework for Engineering Analysis (CAFEAN) Preprocessor Plug-in Application Programming Interface (NUREG/CR-6974, Vol. 1)
- [10] Elkin, I.V., Lipatov, I.A., Antonova, A.I., Nikonov, S.M., Dremin, G.I., Kapustin, A.V., 2004. Single-phase Performance Characteristics of the PSB-VVER Pump, PSB VVER REPORT No. PSB-19.
- [11] Elkin, I.V., Lipatov, I.A., Antonova, A.I., Dremin, G.I., Berezutskaya, M.A., 2003. Report about PSB-VVER hydraulic losses, PSB-VVER REPORT No. PSB-05.
- [12] Elkin, I.V., Dremin, G.I., Lipatov, I.A., Galchanskaya, S.A., 2003. Report about PSB-VVER heat losses, PSB-VVER REPORT No. PSB-04.
- [13] Varju, T., Aranyosy, Á., Orosz, R., Holl, V., Hajas, T., Aszódi, A., 2021. Analysis of the IAEA SPE-4 small-break LOCA experiment with RELAP5, TRACE and APROS system codes, Nuclear Engineering and Design, Volume 377, 111109, June 2021. (<https://doi.org/10.1016/j.nucengdes.2021.111109>)

- [14] Varju, T., Orosz, R., Aranyosy, Á., Holl, V., Hajas, T., Aszódi, A., 2022. Sensitivity analysis of the IAEA SPE-2 small-break LOCA experiment with RELAP5, TRACE and APROS system codes, Nuclear Engineering and Design, Volume 388, 111630, March 2022. (<https://doi.org/10.1016/j.nucengdes.2021.111630>)
- [15] Varju, T., Orosz, R., Kardos, B., Biró, B., Aszódi, A., 2024. Analysis of a PSB-VVER small break LOCA experiment with APROS and TRACE system codes, Annals of Nuclear Energy, Volume 206, 2024, 110662, ISSN 0306-4549, <https://doi.org/10.1016/j.anucene.2024.110662>.
- [16] Bovalini, R., D'Auria, F., Leonardi, M., 1992. Qualification of the Fast Fourier Transform based methodology for the quantification of thermalhydraulic code accuracy, DCMN Report, NT 194 (92), Pisa.
- [17] Prošek, A., Mavko, B., 2003. A tool for quantitative assessment of code calculations with an improved fast Fourier transform based method. Elektrotehniski Vestnik /Electrotechnical Review 70 (2003), 291–296
- [18] Prošek, A., Mavko, B., 2009. Quantitative Code Assessment with Fast Fourier Transform Based Method Improved by Signal Mirroring. International Agreement Report (NUREG/IA-0220)
- [19] D'Auria, F., Galassi, G.M., Belsito, S., Ingegneri, M., Gatta, P., 1997a. UMAE application: Contribution to the OECD/CSNI UMS Vol. 2. DCMN Report, University of Pisa, NT 307(97) Rev. 1.

BIBLIOGRAPHIC DATA SHEET

(See instructions on the reverse)

NUREG/IA-0557

2. TITLE AND SUBTITLE

TRACE Nodalization Performance in PSB-VVER SB-LOCA Benchmark

3. DATE REPORT PUBLISHED

MONTH

July

YEAR

2025

4. FIN OR GRANT NUMBER

5. AUTHOR(S)

R. Orosz, T. Varju, B. Biró & A. Aszódi

6. TYPE OF REPORT

Technical

7. PERIOD COVERED (Inclusive Dates)

8. PERFORMING ORGANIZATION - NAME AND ADDRESS (If NRC, provide Division, Office or Region, U. S. Nuclear Regulatory Commission, and mailing address; if contractor, provide name and mailing address.)

Budapest University of Technology and Economics
Institute of Nuclear Techniques
Műegyetem rkp. 3.
1111 Budapest, Hungary

9. SPONSORING ORGANIZATION - NAME AND ADDRESS (If NRC, type "Same as above", if contractor, provide NRC Division, Office or Region, U. S. Nuclear Regulatory Commission, and mailing address.)

Division of Systems Analysis
Office of Nuclear Research
U.S. Nuclear Regulatory Commission
Washington, D.C. 20555-0001

10. SUPPLEMENTARY NOTES

A. Hsieh, NRC Project Manager

11. ABSTRACT (200 words or less)

In the recent decades computer code calculations have become invaluable in nuclear engineering. With the modern tools, the experts are able to predict the different processes with high accuracy, which has numerous advantages, such as improved reactor safety, enhanced design optimization and cost-effectiveness. It is however essential that the user possesses adequate knowledge and experience about the given code, including its principles and limitations.

In the current report the focus is on the nodalization of the thermal-hydraulic models built for the PSB-VVER integral test facility. Altogether three models have been constructed in TRACE, where the main differences are in the used components and their nodalization of the RPV section. To assess the behavior of the models, a cold leg small break loss of coolant accident benchmark was chosen. In the report we present both the qualitative and quantitative comparison of the calculations and the measurements performed on the facility. For the quantitative evaluation, two methods, namely FFTBM-SM and SARBM, have been used. Finally, a summary of the notable observations and recommendations is included.

12. KEY WORDS/DESCRIPTORS (List words or phrases that will assist researchers in locating the report.)

PSB-VVER
SBLOCA
TRACE
THERMAL-HYDRAULICS
NODALIZATION
FFTBM-SM
SARBM

13. AVAILABILITY STATEMENT

unlimited

14. SECURITY CLASSIFICATION

(This Page)

unclassified

(This Report)

unclassified

15. NUMBER OF PAGES

16. PRICE



Federal Recycling Program



**UNITED STATES
NUCLEAR REGULATORY COMMISSION**
WASHINGTON, DC 20555-0001

OFFICIAL BUSINESS



NUREG/IA-0557

TRACE Nodalization Performance in PSB-VVER SB-LOCA Benchmark

July 2025